CHAPTER 14

Formation Process and Structure of Self-Assembled Monolayer of Thiols in Solution

Ryo Yamada[1], Kohei Uosaki[2]

[1]*Division of Material Physics, Graduate School of Engineering Science, Osaka University, Machikaneyama-1-3, Toyonaka, Osaka 560-8531, Japan*
[2]*Division of Chemistry, Graduate School of Science, Hokkaido University, N10W8, Sapporo, Hokkaido 060-0810, Japan*

CONTENTS

ISBN: 1-58883-082-9

Bottom-Up Nanofabrication
Edited by Katsuhiko Ariga and Hari Singh Nalwa
Volume 3: Pages: 375–394

1. INTRODUCTION

The construction of well-defined surfaces and interfaces is one of the key steps in material science because electronic properties and chemical reactivity of materials are influenced by characteristics of surfaces [1, 2]. The adsorption of a single atomic and molecular layer, i.e., a monolayer, is known to change the surface characteristics, and surface structure should, therefore, be controlled at the level of single molecular thickness. The formation of an organic monolayer is an attractive way to modify or *functionalize* the surface because various combinations of functional groups can be attached and integrated in a single molecule. To realize surface functionalization via molecules, methods to form organic monolayers with controlled orientation and arrangement are required.

In general, molecules spontaneously adsorb on clean surfaces to lower the surface free energy. This surface reaction can be intentionally used to form monolayers. A functional group that possesses a strong and specific affinity for a substrate is used as an anchor. When appropriate molecular–molecular and molecular–surface interactions are present, an ordered monolayer is formed spontaneously (Fig. 1) [3, 4]. This process is called self-assembly (SA).

Monolayers formed in this manner are called self-assembled monolayers (SAMs). It is possible to design interfaces with the thickness of a single molecule and controlled molecular orientations by using SAMs. Table 1 shows a list of typical combinations of functional groups and substrates known to form SAMs. The comprehensive list of the combinations is shown in the references [36]. SAMs are now widely used to control surface properties and electron transfer processes and to stabilize nanoclusters.

Alkanethiol SAMs formed on gold surfaces have been the most widely studied systems. While monolayer formation of thiols on metal surfaces has been known for a long time, the concept of SAM was proposed by Nuzzo et al. in the early 1980s [37]. Significant progress has been made in basic characterization and applications of SAMs in the last two decades [38–43].

SAMs of alkanethiols are formed in various environments such as ultra high vacuum (UHV) [44, 45], gas [46–48], and solution [37], and there seems to be no significant differences in the structures of monolayers formed in different environments. Formation from the solution phase is the most practical and widely used way because even molecules of high molecular weight with small vapor pressure can be used to form a SAM. Typically, a several millimolar solution of alkanethiols in organic solvents such as ethanol and hexane is used to form SAMs.

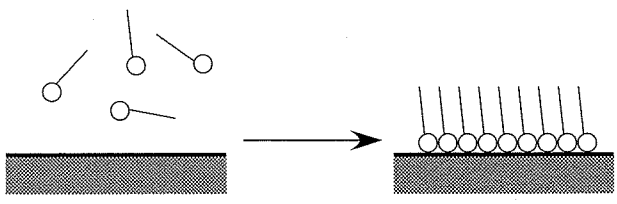

Figure 1. Spontaneous formation of a monolayer on a clean surface.

Functionality of monolayers has been demonstrated by using alkanethiol SAMs as model systems on gold surfaces. Wetting control is one of the simplest and most impressive examples, showing the effect of the monolayer. By choosing the top-most terminal functional group, which is exposed to the surface, the wetting of the gold surface can be controlled from extremely hydrophobic (CH_3) to hydrophilic (COOH) [49]. It is also possible to *switch* the surface wetting property by using reversible photochemical and electrochemical reactions of the terminal group [50–54].

Remarkable examples of SAM applications can be seen in the field of electrochemistry. In the electrochemical process, electrons move from the electrode to the molecule and vice versa. The distance between redox species and the electrode can be controlled by growing organic monolayers on the electrode surface. The electron transfer rate through the molecule, which is an essential parameter in photochemistry, photobiochemistry, and molecular electronics, can be deduced from results of electrochemical analysis of the SAM-modified electrode. The SAMs of alkanethiols provide almost perfect monolayers for this measurement, and the electron transfer rate through an alkyl chain has been determined by using conventional electrochemical instruments [55–59].

The establishment of a well-ordered monolayer has enabled researchers to design more complex electron transfer systems. One of the outstanding examples is the construction of the so-called uphill electron transfer system realized by coupling photoactive (phorphyrin) and electron-relay (ferrocene) groups in a single molecule [60].

Table 1. Combinations between head groups and substrates known to form SAMs via covalent bond formation. Si-H and Si-X represent a silicone surface terminated by hydrogen and halogens, respectively.

Head group	Substrate
SH	Au,[5] Ag,[5] Cu,[5] Hg,[6] GaAs,[7] ITO[8,9]
SeH	Au[10–12]
SCN	Au[13,14]
$SiCl_3$ or $Si(OR)_3$	SiO_2,[15] Al_2O_3,[16,17] Au,[17] ITO[18]
C=C	Si-H,[19] Si-X,[20] Ge-H[21]
CMgBr	Si-H,[22] Si-X,[23–25] Ge-X[26–29]
CLi	Si-H,[30,31] Si-X[23]
$N{\equiv}N^+$	Si-H[32]
N≡C	Pt,[33,34] Au,[35] Pd[35]

Molecular recognition, especially chiral recognition, is a novel application potentially realized by monolayers. In addition to utilizing the specific host–guest interaction between individual molecules, preparation of a surface possessing chiral structures, i.e., a chiral surface, is of great interest. It has been demonstrated that the SA of chiral molecules, e.g., (*R*)- and (*S*)-1,1′-binaphthalene-2,2′-dthiol, is useful for preparing the chiral surface [61].

It is essential to understand the SA process of alkanethiols to design the structure of SAMs. In early studies on the SA process, *ex situ* analytical methods were used. The phase evolution was discovered as a function of coverage in UHV conditions.

Recent progress in analytical methods such as scanning probe microscopy (SPM), quartz crystal microbalance (QCM), optical spectroscopy, and diffraction techniques has enabled us to see *what happens in solutions in real time* with molecular resolutions [62]. Various *in situ* analytical methods have been used to analyze the SA process in solutions.

In this chapter, we review studies on *in situ* observation of the SA process of alkanethiols after giving brief summaries of the preparation methods and basic characteristics of alkanethiol SAMs. Among the many studies using *in situ* analysis, we focus on studies using QCM and scanning tunneling microscopy (STM) because results of those studies contributed significantly to the understanding of kinetics and structural evolution of the SA process, respectively. Readers interested in results of studies using other *in situ* and *ex situ* techniques and in other aspects of SAMs should refer to other articles and books [39–43].

2. PREPARATION METHODS OF ALKANETHIOL SAMS

2.1. Introduction

The preparation of a clean surface is the most important and difficult step because *any* molecules can adsorb on a clean surface. In addition to the surface itself, the environment should be kept clean. In this section, methods for preparing substrates, cleaning tools, and forming SAMs of alkanethols are described.

2.2. Preparation of Substrates

An atomically flat and ordered surface is required for the study of SAMs. A (111)-oriented gold thin film is the most widely used substrate since it is stable in ambient conditions and can be easily formed on various substrates, such as a mica [63–66], glass slide, and silicon [67, 68], by thermal vacuum evaporation. It is worth mentioning that the Au(111) phase can be grown on a polished surface of polycrystalline gold [69]. Grains having atomically flat (111) terraces are grown when the substrate is heated around 300°C during the deposition. Flame annealing is also employed to obtain flat and wide (111) terraces [62].

An adhesive layer is usually required between the gold film and the substrate since adhesion of a gold film to glass and silicon is weak. Thin films of Cr and Ti are typically used as adhesive layers. It should be noted that Cr is known to migrate to the surface of a gold film [70–73]. An organic monolayer of mercaptotrimethyoxysilane is sometimes used as a molecular-adhesive layer to prevent metal contamination of a gold film [74–77].

The (111)-oriented films of other materials such as silver can also be grown by thermal evaporation or sputtering with heating of the substrate during the deposition process [67]. Surface oxidation of materials other than gold is a serious problem for handling the surface in air. Flame annealing and chemical etching are employed to remove an oxide layer. The surface should be treated in an inert gas such as Ar and N_2.

Single crystals are required for studies on specific crystal faces other than (111). The so-called Cravilier or flame-melting method is employed to grow small (a few mm in diameter) single crystals [78, 79]. When a polycrystalline metal wire, such as gold, silver, platumum, palladium, or Rh, is melted by a flame, a small molten metal bead dangles on the edge of the wire. The molten metal bead is solidified to a single crystal by very gentle cooling as shown in Figure 2(a). Small facets of (111) and (100) surfaces appear on the single crystal bead as shown in Figure 2(b, c). The orientation of a single crystal can be determined from the positions of the facets. A surface with a desired orientation is obtained by cutting the crystal. The facet itself is very flat and is a good

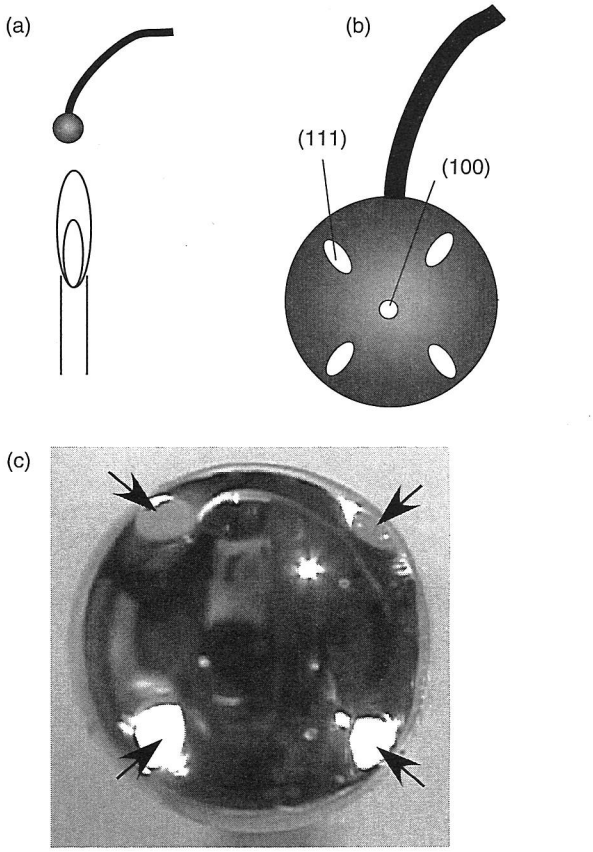

Figure 2. Method to make a single crystal bead formed by a flame-melting method. (a) An edge of polycrystalline wire is melted to form a bead and cooled very gently. (b) A schematic drawing showing facets appeared on a single crystal bead. (c) A photograph of a single crystal bead of gold formed by a flame-melting method. (111) facets are indicated by arrows. The diameter of the bead is ca. 3 mm.

substrate for STM measurement. Electrochemical epitaxitial growth on gold surfaces is useful for preparing well-defined surfaces of various metals, such as platinum and palladium [80–83].

2.3. Cleaning of Tools and Surfaces

Since SAMs are usually grown in solution phases as mentioned before, tools such as vessels and tweezers used to prepare the solution should be cleaned very carefully. A typical cleaning procedure is as follows.

(1) Immerse the glass vessel in concentrated H_2SO_4 overnight or in *piranha* solution (1:3 mixture of H_2O_2 and H_2SO_4) for tens of minutes.
(2) Rinse the glass vessel with doubly deionized water.
(3) Rinse the glass vessel again with hot doubly deionized water to remove residual H_2SO_4.
(4) Rinse with ethanol and then with the solvent that will be used to prepare the SAM solution.

It is better not to dry the vessel since contaminants in air can easily absorb to the vessel wall. A liquid layer can prevent the surface from being contaminated. Metal tweezers are not suitable because they cannot be rigorously cleaned in the same way.

Surface contaminants should be removed from the substrate surface just before the modification of molecules. Usually, organic materials are the major contaminants disturbing the SAM formation. In the case of gold substrates, contaminants can be easily removed by oxidation without causing serious damage to the surface itself. Typically, substrates are immersed in a concentrated H_2SO_4 or *piranha* solution. UV-O_3 cleaning and flame annealing are also used. An alkaline solution, e.g., 1 M KOH in ethanol, is an alternative choice to remove organic contaminants from the surface. Since the top-most layer of the gold surface may be damaged by chemical oxidation, the surface is subjected to flame or thermal annealing to recover the reconstructed surface just before use.

2.4. Formation of SAMs

Typically, solutions of several millimolar thiol molecules in organic solvents such as ethanol, hexane, dichloromethane, and toluene are used for the preparation of SAMs. Most of the commercially available chemicals are usually used without further purification, though residual impurity of sulfur is known to disturb the formation of an SAM of pyridinethiol on a Au(111) surface [84]. To form a monolayer, a clean substrate is immersed in the solution for 1–24 h. Sometimes, a much longer period, such as several days, is required for completion of the monolayer formation [85]. It is known that a clean surface can be maintained in pure liquids. This is one of the advantages of using a solution to form SAMs. While the concentration of the solution does not seem to have a strong effect on the final structures of monolayers, temperature and solvent strongly affect the density of the defects and domain size [86, 87]. These effects are discussed in the following section.

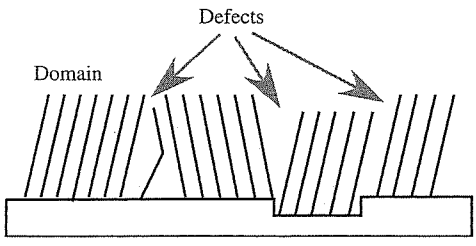

Figure 3. Schematic model for the realistic monolayer structure including an ordered domain, conformational/orientational disorder, and surface reconstruction of the substrate.

Table 2. Methods to characterize monolayers.

Interest	Methods
Chemical composition	Contact angle,[37, 49, 88] IR,[89] XPS[88]
Thickness	Ellipsometry,[88] SPR,[90, 91] AFM,[92] XPS[93]
Molecular orientation	IR[89]
Molecular arrangement	SXRD,[40, 94, 95] LEED,[96] STM[42, 97, 98]
Packing density	Electrochemistry,[55–59, 99] QCM,[100, 101] STM
Defect structure	STM, AFM,[102] Electrochemistry
Coverage	STM, QCM, Electrochemistry, SPR

3. ANALYTICAL METHODS

3.1. Introduction

Figure 3 shows a schematic model of a realistic monolayer structure including defects. In the ordered domains, a single crystalline-like structure is formed. Positions of molecules with respect to substrate atoms are determined by interactions between an anchoring group and substrate atoms. Structures of single crystals of molecules are usually helpful to understand those of monolayers, since molecular packing structures are determined by interactions among molecular frameworks. In the case of the SAMs of alkanethiols on Au(111), the molecular axis is known to be tilted by ca. 30° from the surface normal to achieve close packing of molecular skeletons similar to single crystals of alkanes.

Variable molecular conformations and tilt directions are one of the origins of defects. Size and distribution of these defects might be related to the growth process of a monolayer. For example, when a monolayer grows in an island-formation process from particular nucleation sites, defects are likely to be formed where two islands meet. Structures of a substrate before and after monolayer formation are also of interest because adsorption of molecules can alter atomic arrangement of surfaces.

Table 2 summarizes methods to characterize monolayers. Optical spectroscopy and scanning probe microscopy play major roles in the analysis of organic monolayers since organic monolayers can be easily damaged by an electron beam. It is worth noting that electrochemistry provides fruitful information on structures of monolayers by simple measurements.

In this section, several techniques used to analyze the structure of SAMs are briefly described. Readers who would like to know more details and other techniques should consult the references [3, 39–43].

3.2. Simple Test for Monolayer Formation

Monolayer formation can be easily checked from contact angle measurement when the surface energy is qualitatively predictable. Kinetics of the monolayer formation is also qualitatively measurable since the contact angle is known to change as a function of coverage [37, 49, 88]. It should be noted that contact angles are sensitive not only to chemical composition but also to surface roughness and molecular order [103]. Conformational change [52, 53] and chemical reactions of terminal functional groups of monolayers can also be detected by change of the contact angle [50, 51, 54].

Of course, the contact angle *cannot* prove that the surface is covered with a monolayer, i.e., the surface can be covered with a multilayer or just contaminants.

3.3. Thickness

Thickness of the film is an essential parameter to characterize a monolayer. When the thickness of the film is smaller than the length of the molecule, it is assumed that the molecules are tilted in the monolayer or that full coverage has not been achieved. On the other hand, when the thickness is larger than the length of the molecule, a multilayer has been formed. Ellipsometry is the standard technique to measure the thickness of a monolayer [1]. Surface plasmon resonance spectroscopy (SPR) [90, 91] and angle-resolved X-ray photoemission spectroscopy (XPS) [93] are also employed. Thickness can also be measured by scratching the surface by atomic force microscopy (AFM).

3.4. Chemical Composition

Infrared spectroscopy (IR) is usually used to identify the functional groups in the monolayer. The orientation of the functional groups with respect to the surface plane can also be deduced. Techniques to measure an IR spectrum of a monolayer are described below.

XPS is used to measure atomic composition of the surface. Since carbon and sulfur are major contamination sources in air, these elements are not suitable for the analysis. Angle-resolved XPS reveals the order of functional groups normal to the surface.

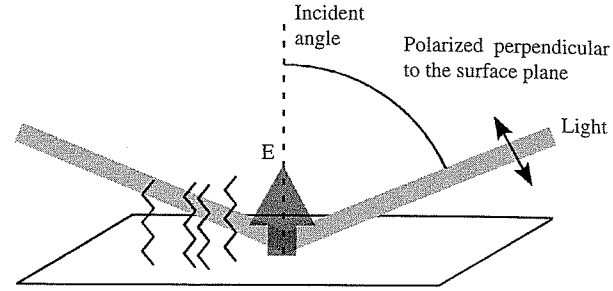

Figure 4. Schematic illustration of a grazing-angle FTIR experiment.

Figure 5. Schematic diagram of the optical path for reflection–absorption measurement of the monolayer.

When a redox group is attached to the molecules, electrochemical measurement can be employed to detect the existence of the redox group [85].

3.5. Molecular Order and Orientation

Vibrational spectroscopy provides useful information on composition, crystallinity and orientations of molecules in a monolayer. Various techniques for detecting weak absorption by monolayers have been developed [3].

Grazing angle reflection absorption IR spectroscopy utilizes p-polarized (polarized perpendicular to the surface plane) light, which effectively couples with vibrational modes of molecules perpendicular to the surface plane [104] as shown in Figure 4. The incident angle of the IR beam should be large to obtain signals from monolayers [105]. The reflection is multiplied to increase the signal-to-noise ratio by coupling two gold substrates in face-to-face as shown in Figure 5 [106].

Polarization-modulation (PM)-IR spectroscopy utilizes the difference in sensitivity of *p*- and *s*-polarized light to

Table 3. Peak positions of CH_2 and CH_3 vibrational modes in various phases. Reprinted with permission from [112], M. D. Porter et al., *J. Am. Chem. Soc.*, 109, 3559 (1987). © 1987, American Chemical Society.

Structural group	C—H stretching mode	Peak positions[a] for crystalline and liquid states, cm^{-1}		Peak positions[a] for $CH_3(CH_2)_nSH$ adsorbed at gold, cm^{-1}							
		Crystalline[b]	Liquid[c]	$n=21$	$n=17$	$n=15$	$n=11$	$n=9$	$n=7$	$n=5$	$n=3$
$-CH_2-$	ν_a	2918	2924	2918	2917	2918	2919	2920	2921	2921	*d*
	ν_s	2851	2855	2850	2850	2850	2851	2851	2852	2852	*d*
CH_3-	ν_a(ip)	*e*	*e*	2965	2965	2965	2965	2966	2966	2966	2966
	ν_a(op)	2956	2957	*f*	*f*	*f*	*f*	*f*	*f*	*f*	*f*
	ν_s(FR)	*g*	*g*	2937	2938	2938	2937	2938	2939	2939	2938
	ν_s(FR)	*g*	*g*	2879	2878	2879	2879	2878	2879	2878	2877

[a]Peak positions are determined as the average for four independent spectra and are accurate to within 1 cm^{-1}. Corrections for optical dispersion distortion effects of an equivalent reflection spectrum for a monolayer are less than 1 cm^{-1} for all peaks. Further details are pointed to in the text. [b]Crystalline-state positions determined for $CH_3(CH_2)_{21}SH$ in KBr (see text). [c]Liquid-state positions determined for $CH_3(CH_2)_7SH$ with a liquid prism cell (see text). [d]Peak position could not be accurately determined because of low signal-to-noise ratio. [e]The ν_a(ip) is masked by the strong ν_a(op) in the crystalline- and liquid-state spectra. [f]The position for ν_a(op) cannot be determined because of the low signal-to-noise ratio. This is a result of the orientation of this mode with respect to the surface. [g]Both ν_s(FR) bands are masked by the $\nu_a(CH_2)$ band.

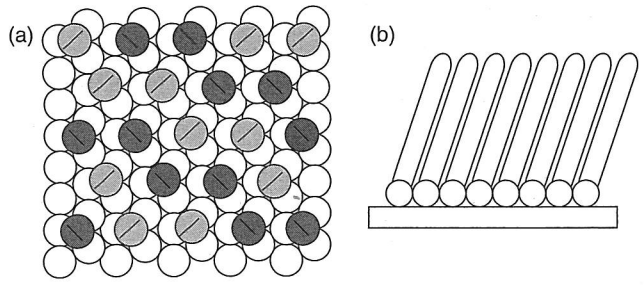

Figure 6. (a) Model of molecular arrangement (shadow circle) with respect to the Au(111) surface (open small circle). The diagonal slash indicates the azimuthal orientation of the plane defined by the C-C-C backbone of an all-trans hydrocarbon chain. (b) Side view of the molecules. Circles represent sulfur atoms.

surface [107–109]. The intensity of absorption changes when the polarization of light is changed from *p* to *s* because *s*-polarized light is almost insensitive to the surface. The difference between the spectra of *s*- and *p*-light can be precisely measured by a lock-in technique. The advantage of the PM-IR method is that a reference signal is not required to obtain absorption spectra.

Attenuated total reflection (ATR) IR spectroscopy utilizes an evanescent light, which is generated on a surface when a light is totally reflected [110, 111]. Usually, a prism made of silicon or germanium is used to obtain evanescent IR light. Absorption of the evanescent light decreases intensity of the reflected light. Changes in spectra of the reflected light therefore represent the absorption in the evanescent light field. Since the evanescent light propagates only several hundreds of nm from the surface, ATR-IR is sensitive to the surface layer. ATR-IR is especially preferred when a monolayer is grown directly on a prism surface.

Molecular orientation is estimated by considering the relationship between polarization of a light and direction of molecular vibrations on a surface. When *p*-polarized light is reflected with a large incident angle, vibration modes perpendicular to the surface plane are effectively excited because the excited electric field is almost perpendicular to the surface plane. As the vibration moment tilts from the surface normal, the absorption becomes weaker. The relative peak intensity is compared to that obtained in a spectrum of a liquid phase in which random orientations of the molecules is expected, and the orientation of the molecules is quantitatively calculated.

Crystallinity of alkyl chains in monolayers is discussed from the peak positions of CH_2 and CH_3 vibration modes of alkyl chains since these peaks are known to shift to higher frequencies as a phase transition proceeds from solid to liquid as shown in Table 3 [112].

Sum frequency generation (SFG) spectroscopy is a very powerful technique to measure vibrational spectra of monolayers since SFG light is generated only at the interface where the asymmetric structure exists [113–115]. Interestingly, SFG sometimes cannot detect CH_2 vibration of SAMs consisting of long alkyl chains because the molecular skeleton of an alkyl chain is almost symmetric in the closely packed monolayer. Thus, SFG spectra in the CH region can be used to probe the conformational order of the SAM.

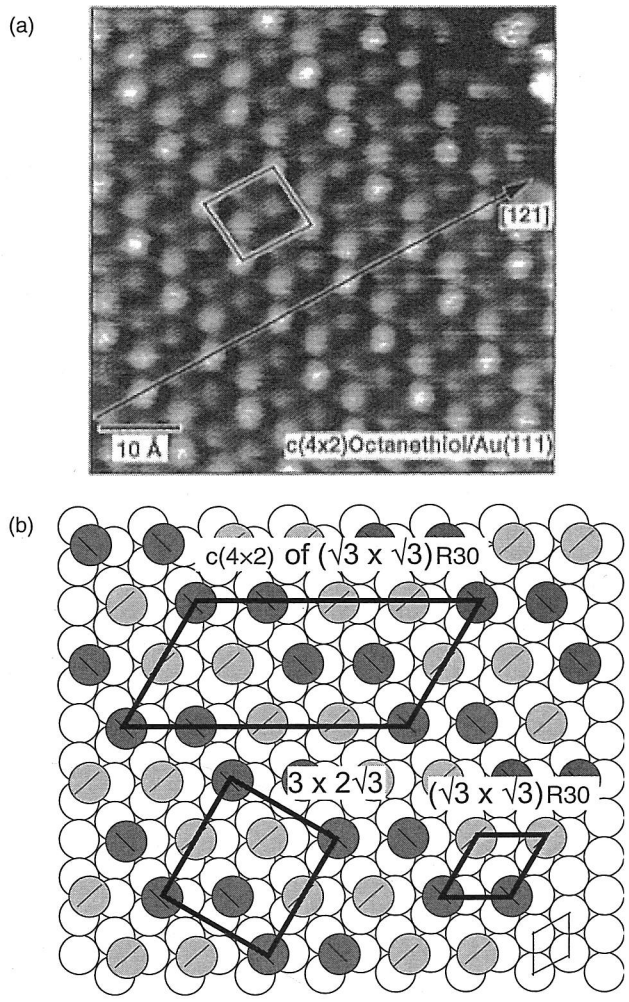

Figure 7. (a) STM image of a Au(111) surface covered with an octanethiol monolayer. The rectangular cell represents the unit cell for $3 \times 2\sqrt{3}$. Reprinted with permission from [98], G. E. Poirier and M. J. Tarlov, *Langmuir* 10, 2853 (1994). © 1994, American Chemical Society. (b) Unit cell structures representing thiol molecular arrangement. When the direction of the alkyl chain is ignored, the molecular arrangement is $(\sqrt{3} \times \sqrt{3})R30°$.

3.6. Molecular Arrangement

Molecular arrangements of SAMs are measured by electron diffraction [96], grazing-incidence X-ray diffraction (GIXD) [94, 95], and He atom diffractions [94]. Electron diffraction and He atom diffractions are sensitive to the order of the terminal group exposed to the surface, while GIXD detects the order of the positions of thiols. Organic monolayers are, however, easily damaged by probes such as an electron beam and X-rays [116].

SPMs such as STM and AFM enable visualization of the molecular arrangement and individual molecules on surfaces in vacuum, air and solutions [117–120].

A high tunneling gap impedance, i.e., small tunneling current and high bias voltage, is required for observation of SAMs of alkanethiols by STM to avoid penetration of the tip into the monolayer [42, 97, 98]. The longer the alkyl chain is, the smaller the tunneling current should be. Typical imaging conditions are several pA of tunneling current and

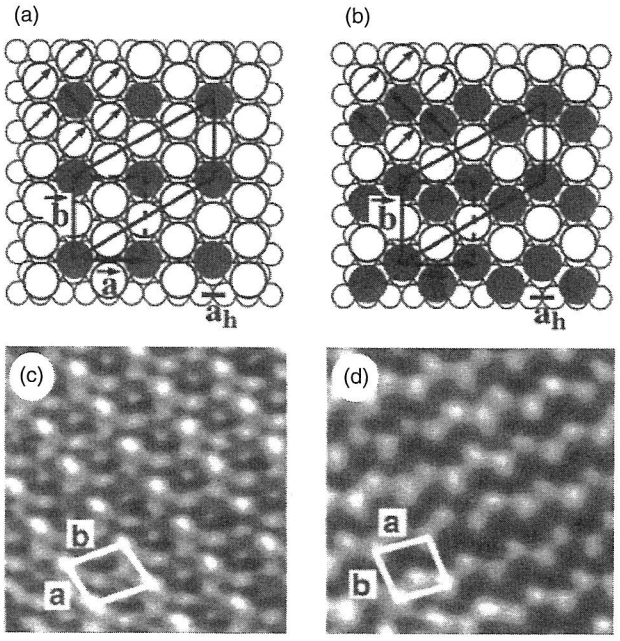

Figure 8. Other kinds of $c(4 \times 2)$ of $(\sqrt{3} \times \sqrt{3})R30°$ observed in STM measurement. (a) and (b) represent models of the STM images shown in (c) and (d). Reprinted with permission from [97], E. Delamarche et al., *Langmuir* 10, 2869 (1994). © 1994, American Chemical Society.

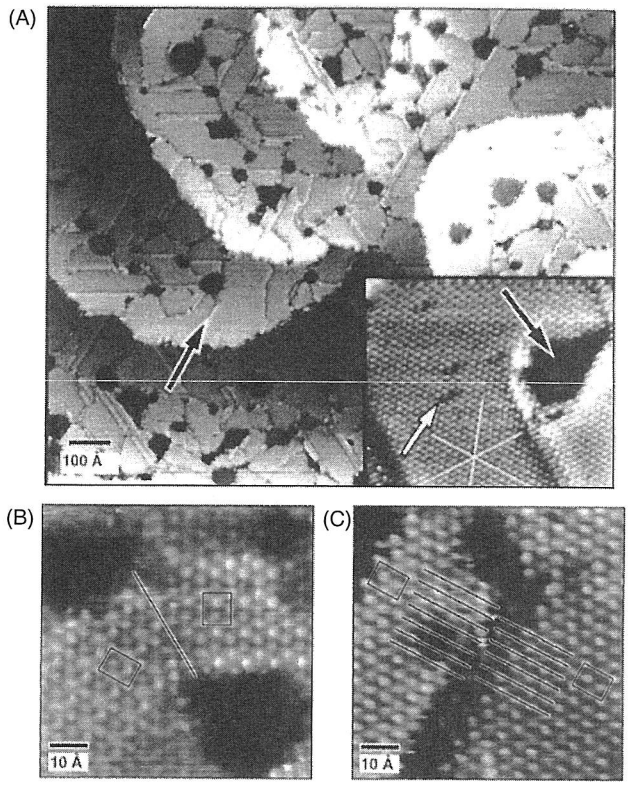

Figure 9. (A) Wide STM image of the Au(111) surface covered with a dodecanethiol monolayer. (B) and (C) represent orientational and translational domain boundaries, respectively. Reprinted with permission from [42], G. E. Poirier, *Chem. Rev.* 97, 1117 (1997). © 1997, American Chemical Society.

0.5–1 V of bias voltage for a decanethiol monolayer formed on Au(111). Molecularly resolved images are relatively easily and reproducibly obtained for a monolayer of alkanethiols with a chain length from $n = 8$ to 12 ($CH_2C_{n-1}H_2SH$).

The noise and leak current in the microscope system are important issues in imaging with high gap impedance. They are affected by humidity and by cleanness of the tip and substrate. Measurements are carried out in inert gas to control humidity.

3.7. Packing Density

When molecular arrangement can be directly imaged by STM, the number of molecules can be easily counted. Unfortunately, imaging of organic monolayers is not always possible.

Electrochemistry is an easy and powerful technique to estimate the number of molecules on a surface when a monolayer is electrochemically active. For example, when the molecule contains ferrocene, the charge required to finish the electrochemical reactions of the ferrocene group can be directly used to estimate the number of the molecules by assuming one electron transfer reaction [55–59].

Even when the SAM carries no redox groups, the number of adsorbed molecules can be determined electrochemically. Alkanethiol SAMs are known to be desorbed when the potential is swept to negative because the thiolate on the surface is reduced [99, 121]. The current due to the reduction of the thiolate is detected in aqueous solution when pH sufficiently is high to prevent the generation of hydrogen. The number of desorbed molecules is estimated from the charge required to complete the reaction. The position and shape of the current peak in a cyclic voltammogram are sensitive to the order in the monolayer and the crystallographic face of the substrate. It should be noted that the charging of the electrical double layer should be carefully taken into account to interpret the data since the double-layer capacitance changes during the desorption of the monolayers.

3.8. Coverage

Coverage of the surface and kinetics of SAM formation are quantitatively measured by using IR, electrochemistry, and QCM. SPR and ellipsometry are also employed, although quantitative interpretation of data is complicated. IR peak intensity is basically proportional to the coverage of molecules if no dynamic orientational change takes place during the adsorption. Electrochemical measurement can be used to measure the number of molecules on a surface as described above.

QCM is a useful technique for determining a surface mass change in the order of nanograms per centimeter squared [122, 123]. Quartz crystal is a piezoelectric material, and mechanical resonance frequency of a quartz plate is measured by using an electric oscillator. When a thin film adsorbs on an electrode attached to the quartz plate, the resonance frequency of the quartz plate changes. The frequency change, Δf, is proportional to the surface mass change, Δm, due to the adsorbed film as follows:

$$\Delta f = -2f_0^2 \Delta m / A(\mu_q \rho_q)^2$$

where f_0 is the frequency of the crystal prior to a mass change, A is the piezoelectrically active area, ρ_q is the density of quartz (2.648 g/cm^3), and μ_q is the shear modulus (2.946×10^{11} g/(cm s)). This relationship is called Sauerbrey's equation. The sensitivity of a 5 Mhz AT-cut crystal is 17.7 ng cm^2/Hz. For example, hydrogen adsorpion on the surface at a density of 10^{15} cm^{-2} causes a change of a frequency by ca. 0.1 Hz. QCM can detect the adsorption of a submonolayer with a reasonable time resolution, since a frequency change of 0.1 Hz is detected within 0.1 s by a conventional frequency counter.

Oscillator circuit diagrams to operate QCM in solutions, i.e., under the condition of strong viscoelastic damping, are available in literature [124]. A Au(111) electrode is grown by thermal evaporation onto a polished quartz plate heated at about 150°C. The temperature of quartz should not exceed 573°C since phase transition of quartz takes place at this temperature.

It should be noted that resonant frequency of a quartz crystal changes not only because of change in mass but also because of change in temperature and viscoelastic properties of the interface [122, 123]. Impedance analysis can clarify origins of the frequency change.

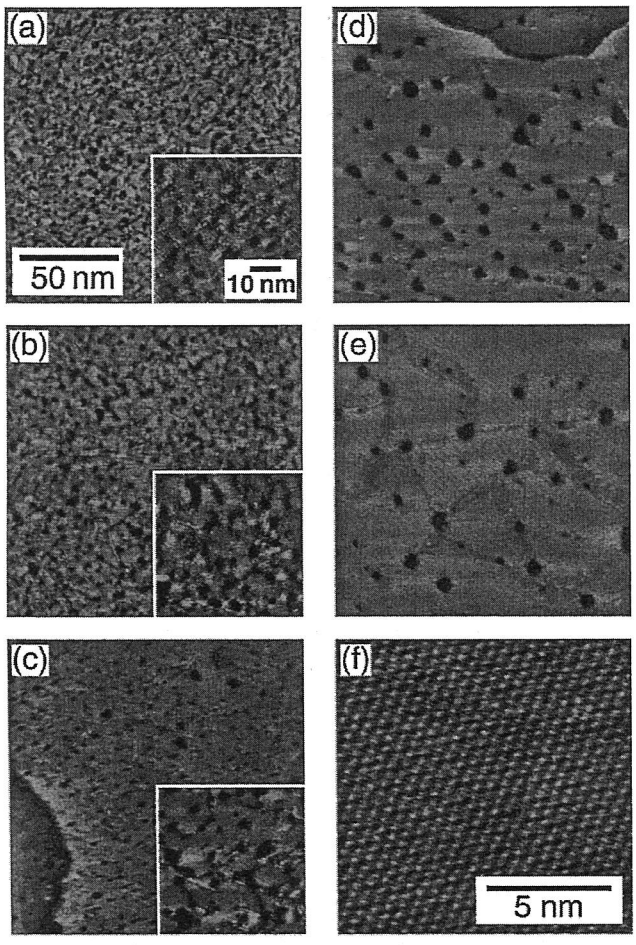

Figure 10. STM images of a Au(111) surface covered with a decanethiol monolayer. Modification was carried out at (a) −20°C, (b) 5°C, (c) 25°C, (d) 60°C, and (e) 78°C (boiling point) in 1 mM solution in ethanol for 1 h. (f) Typical image of molecular resolution. Reprinted with permission from [86], R. Yamada et al., *Langmuir* 16, 5523 (2000). © 2000, American Chemical Society.

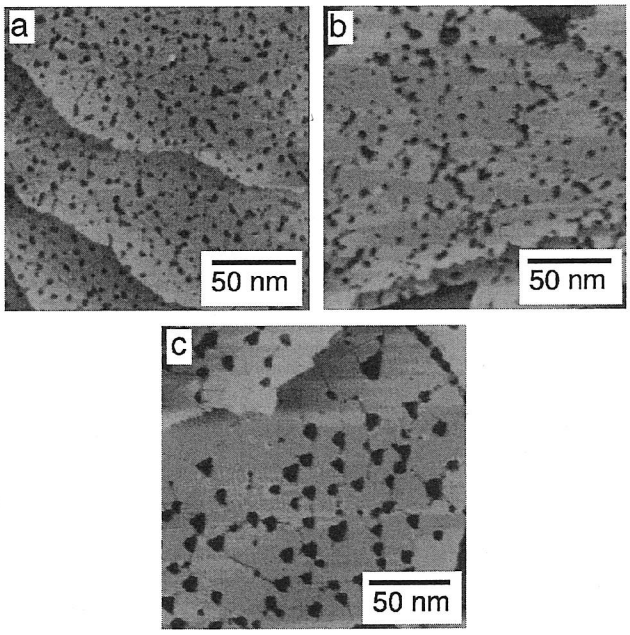

Figure 11. STM images of a Au(111) surface covered with a decanethiol monolayer modified in 1 mM solution in (a) ethanol, (b) DMF, and (c) toluene for 1 h. Reprinted with permission from [87], R. Yamada et al., *Chem. Lett.* 28, 667 (1999). © 1999, American Chemical Society.

3.9. Defect Structure

Monolayers always have defects such as molecular disorder and pinholes. SPM is the most powerful method to characterize defect structures. However, it is sometimes difficult to obtain clear images of the monolayer structure, especially when bulky functional groups are attached at the end of the molecules.

Electrochemistry is useful to detect defects of monolayers. For example, densely packed insulating monolayers prevent the redox species from approaching the electrode. As a result, the electrochemical reactions of the substrate and the redox species in solution are strongly suppressed [112, 125–128]. If there are pinholes in the monolayer, a leak current is observed. When the monolayer possesses redox active functional groups, peak positions and width of the cyclic voltammogram are related to the uniformity of SAMs [129–132].

4. STRUCTURES OF SAMS OF ALKANETHIOLS ON GOLD SURFACES

4.1. Introduction

SAMs of alkanethiols on a Au(111) surface is the most widely studied monolayer system. A well-ordered and solid-like nature of the monolayer was evident from studies using IR [89] and diffraction techniques [133–135]. STM measurements using high gap impedance revealed detailed structures of the alkanethiol SAMs [42].

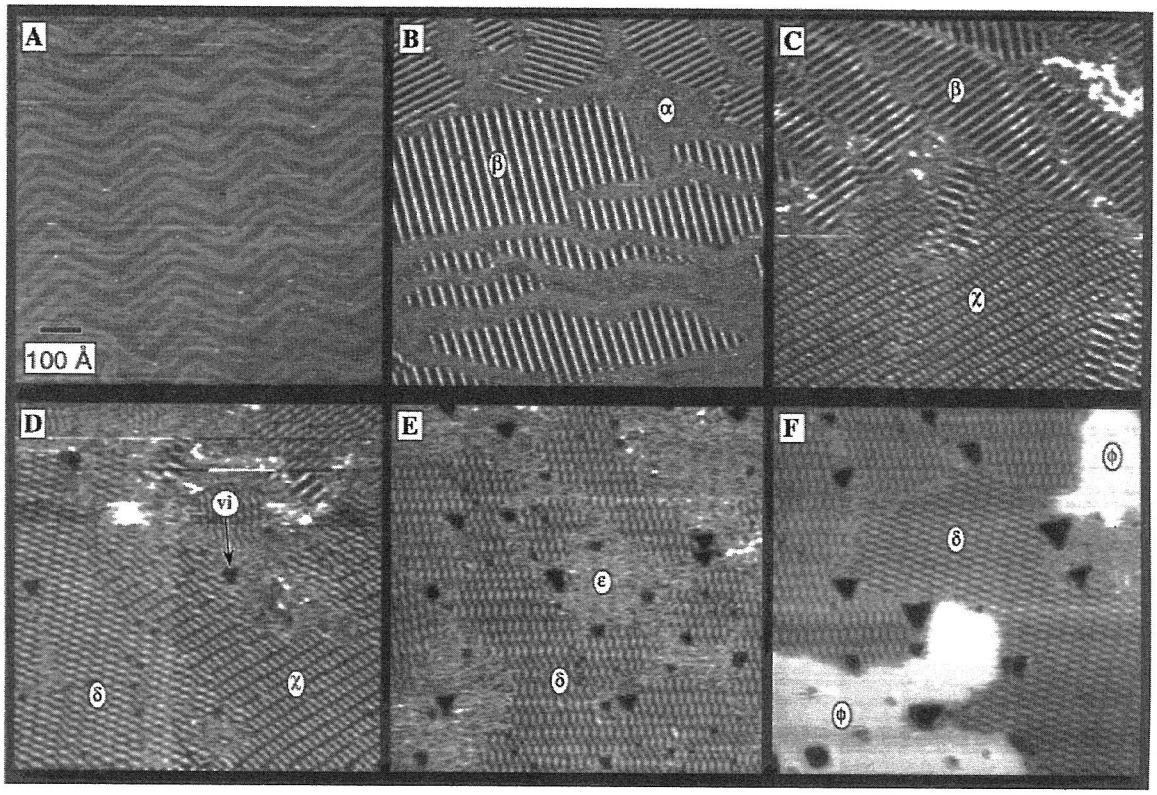

Figure 12. Isothermal growth of decanethiol on Au(111) in UHV conditions at 22°C. (A) Clean Au(111) surface showing herringbone reconstruction. (B) Surface exposed to decanethiol flux. b-phase and two-dimensional gas coexist. (C) b- and χ-phase observed at higher surface coverage. As adsorption proceeded, phases with higher coverage were generated (D, E, F). Reprinted with permission from [160], G. E. Poirier et al., *Langmuir* 17, 1176 (2001). © 2001, American Chemical Society.

One significant finding was the formation of small pits on the surface. It was shown that these pits are not pinholes of the monolayer but depressions formed in the top layer of the gold surface [136–138]. Another major finding was a missing-row-like defect where molecules are absent. The missing rows look like cracks in the monolayer. These structures are discussed in detail below.

These findings show that an alkanethiol SAM is not formed by a simple adsorption of molecules but through dynamic rearrangement of gold atoms and molecules. In fact, there is still controversy in some of the basic aspects such as position of sulfur atoms on the surface [43]. New structures have been reported [139]. In this section, only structures that are widely accepted are reviewed.

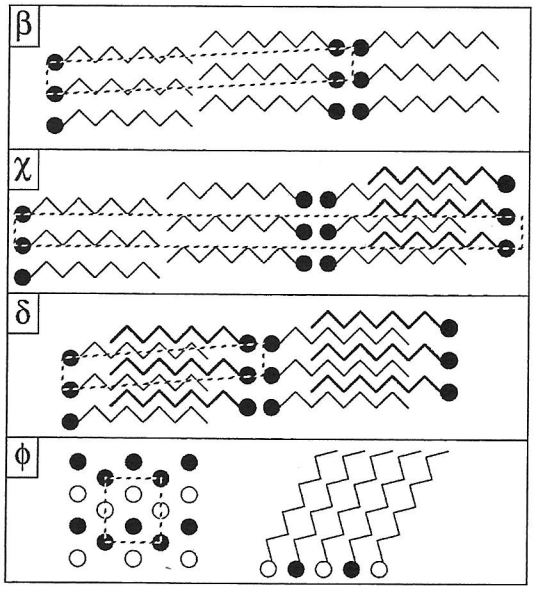

Figure 13. Schematic model of molecular arrangement in various phases. Reprinted with permission from [160], G. E. Poirier et al., *Langmuir* 17, 1176 (2001). © 2001, American Chemical Society.

4.2. Molecular Arrangement of Thiol SAMs on a (111) Surface at Full Coverage

Figure 6(a, b) shows top and side views of a monolayer, respectively. The molecule is located on a threefold site of a gold surface as shown in Figure 6(a). This arrangement is called $(\sqrt{3} \times \sqrt{3})R30°$ with respect to the Au(111) surface since the unit cell length is $\sqrt{3}$-times longer that that of Au(111) and the direction is rotated by 30° as shown in Figure 6(b). The alkyl chain is tilted from the surface normal about 30° with an all-trans conformation. This tilt angle comes from the conditions for close packing of alkyl chains. IR measurement revealed that the plane defined by an all-trans carbon molecular skeleton alternatively changes its direction as shown in Figure 6(a). The arrangement of the molecular skeleton is represented as $c(4 \times 2)$ with respect to the molecular arrangement, i.e., $(\sqrt{3} \times \sqrt{3})R30°$ structure and, and the molecular arrangement of the alkanethiols

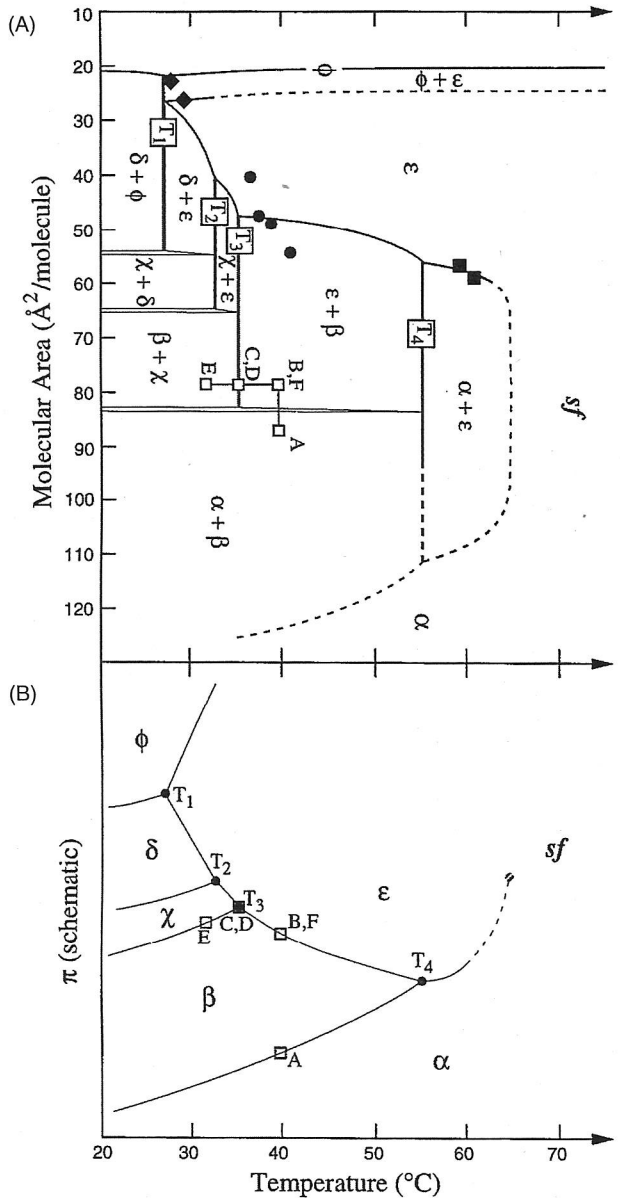

Figure 14. Two-dimensional phase diagram of (A) temperature versus molecular area and (B) pressure versus temperature. Note that surface pressure was not measured. Reprinted with permission from [160], G. E. Poirier et al., *Langmuir* 17, 1176 (2001). © 2001, American Chemical Society.

is sometimes described as $c(4 \times 2)$ of $(\sqrt{3} \times \sqrt{3})R30°$ with respect to Au(111) (Fig. 7(b)).

Figure 7(a) [98] shows a high-resolution STM image. In addition to the $(\sqrt{3} \times \sqrt{3})R30°$ molecular packing structure, small variations in height among the molecules are observed. The structure considering these modulations corresponds to $c(4 \times 2)$ of $(\sqrt{3} \times \sqrt{3})R30°$. Sometimes two kinds of $c(4 \times 2)$ structures are observed by STM [97, 98] and noncontact AFM [140, 141] as shown in Figure 8. One has a square (Fig. 8(a)) and the other has an oblique unit cell (Fig. 8(b)). GIXD analysis showed that only an oblique structure is possible [40, 134, 135]. Although the possibility of polymorphism cannot be ruled out, the convolution effect of the

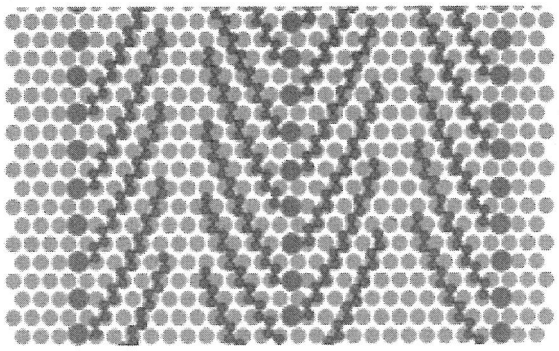

Figure 15. Alternative model for flat-lying phase of alkanethiols. Reprinted with permission from [161], C. Munuera et al., *Langmuir* 21, 8270 (2005). © 2005, American Chemical Society.

unsymmetrical tip is likely to be the reason for the different structures imaged by STM.

One of the origins of the $c(4 \times 2)$ structure is different orientations of the alkyl termination due to different twist angles among alkyl chains [97, 98]. In addition, arrangement of the sulfur atoms is also considered. GIXD measurement showed that the positions of sulfur atoms deviate slightly from hexagonal symmetry, indicating the existence of two kinds of sulfur positions [40, 95]. The different sulfur adsorption sites can result in variable electronic structure and height in the monolayer and can be the origin of the $c(4 \times 2)$ structure.

In fact, the position of the sulfur atom on the gold surface is still under controversy. In early studies, the sulfur atom was believed to be located on a threefold hollow site of gold atoms. However, recent theoretical and experimental results are shown that the sulfur stays on atop [142–144], bridge [145–149], and multiple [95, 150–154] sites.

An STM image of a large area revealed various defect structures as shown in Figure 9(A). One significant feature is a pitlike structure. The depth of the pits is shown to be equal to the monoatomic height of the Au(111) surface, and the molecules are present in the hole [136–138]. Considering

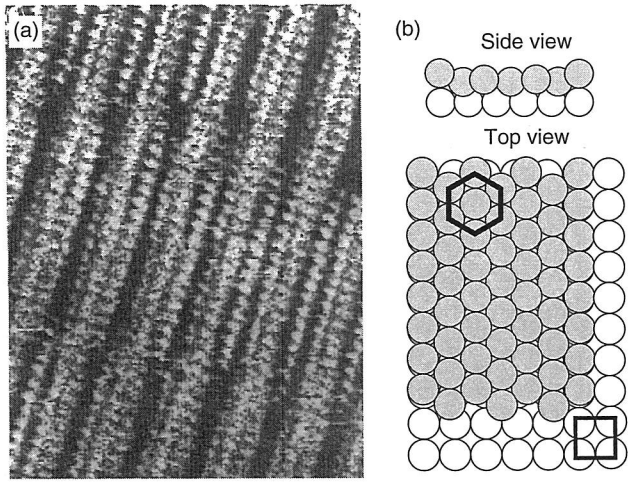

Figure 16. Structure of reconstructed Au(100) surface. (a) STM image. Reprinted with permission from [162], O. M. Magnussen et al., *Surf. Sci.* 296, 310 (1993). © 1993, Elsevier.

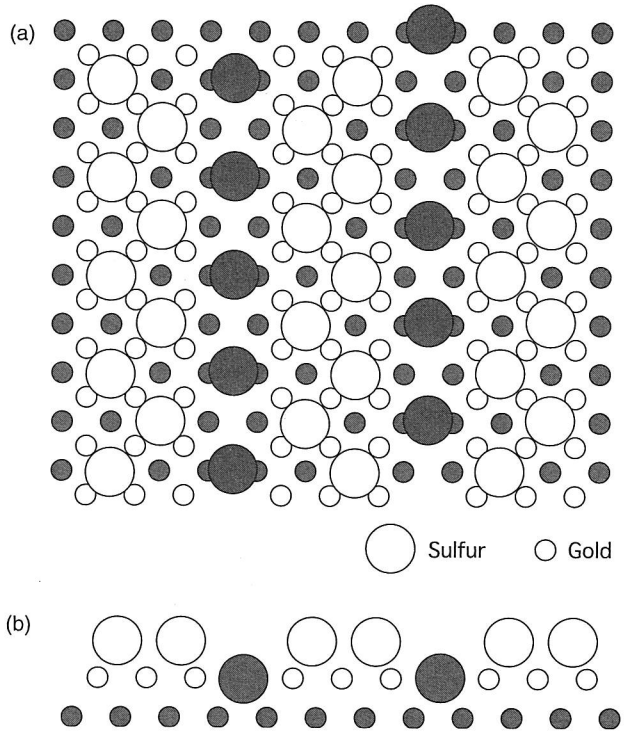

Figure 17. Models of a Au(100) surface covered with a butanethiol monolayer. A top and side view are shown in (a) and (b), respectively. Large open and filled circles are sulfur atoms located on the top-most surface and the missing row of the gold surface, respectively. Small circles represent gold atoms.

these facts, the holes are not pinholes in the monolayer but depressions of the Au surface created during the monolayer formation. These depressions of the Au surface are called vacancy islands (VIs) of gold surface. The VIs are known to be formed at the initial stage of the SA and grow in an ostwald ripening process as discussed in the next section [155, 156].

Origins of VIs are not fully understood. Since shrinking of the gold surface was not detected after monolayer formation, gold atoms seem to be removed from the top layer. One possible reason is dissolution of gold into the solution [136]. This effect seems to have a very small contribution since the total area of the VIs in the unit area of the surface is always constant regardless of the solvent and temperature [86, 87], which are expected to change the etching rate. The extraction of an excess amount of gold atoms might take place when the reconstruction of gold surface is lifted [157].

Other significant structures in STM images are domain boundaries. A domain boundary typically consists of thin void lines with a space of a single molecule or several molecules. These defects originate form misfits in tilt angles, staking geometry and rotational direction of $c(4 \times 2)$ geometry. Figure 9(b, c) shows typical domain boundaries caused by rotational and stacking misfits, respectively.

The grains become larger with increase in temperature during the modification process as shown in Figure 10 [86]. Although the average size of VIs is larger at higher temperature, the number of VIs is less. Consequently, the total area

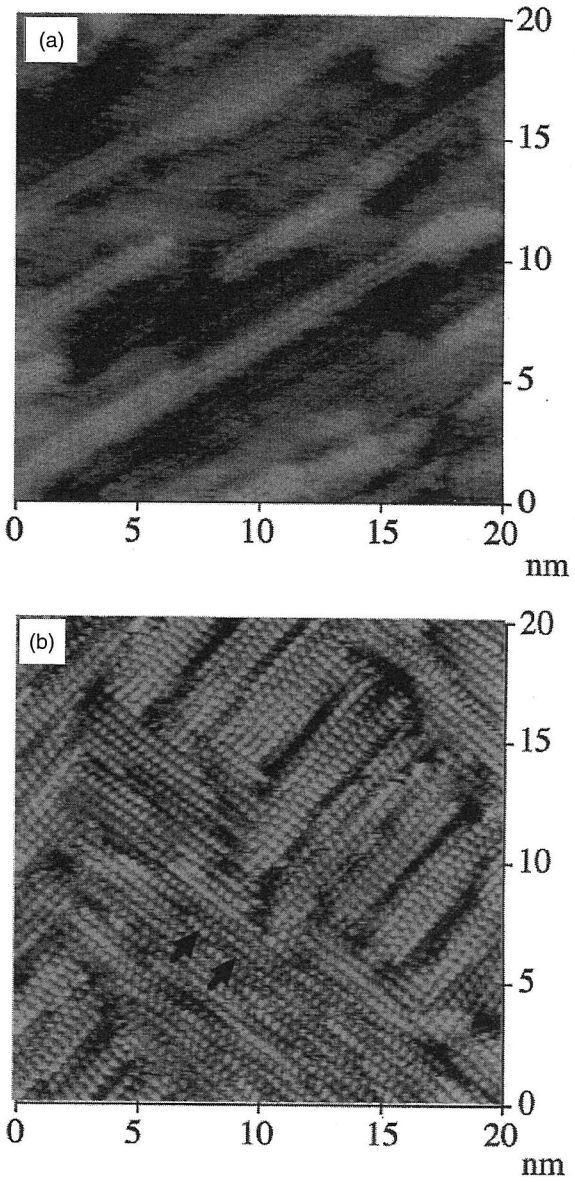

Figure 18. STM images of a Au(100) surface covered with a decanethiol monolayer. Modification was carried out on (a) reconstructed and (b) (1×1) Au(100) surfaces. Reprinted with permission from [168], R. Yamada and K. Uosaki, *Langmuir* 17, 4148 (2001). © 2001, American Chemical Society.

of VIs on the surface is constant regardless of temperature. The total perimeter of the VIs, which represents the total length of the line defects in the monolayer formed at the step of VIs, becomes shorter at higher temperature. A similar effect is obtained by annealing the monolayer [158, 159]. The solvent also has a strong influence on the defect density in SAMs as shown in Figure 11, though the reason for the difference is not clear [87].

4.3. Molecular Arrangement of Thiol SAMs on a (111) Surface at Low Coverage

Poirier and co-workers constructed a phase diagram based on STM investigations in UHV [160]. When the coverage

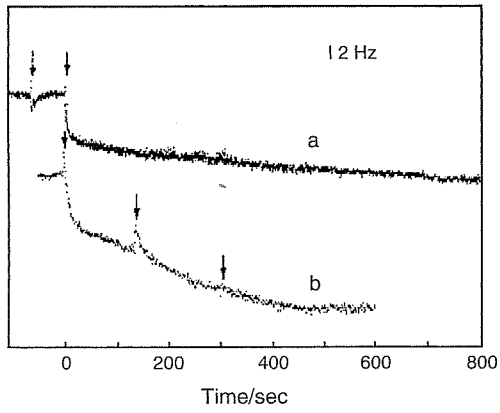

Figure 19. Frequency change during the self-assembly of ferrocenylundecanethiol on a Au electrode formed on QCM in hexane. $FcC_{11}SH$ solution was injected at the solid arrow. (a) and (b) represent the cases of single and multiple injections of $FcC_{11}SH$ solution, respectively. The dotted arrow in (a) represents the injection of pure hexane. Reprinted with permission from [100], K. Shimazu et al., *Langmuir* 8, 1385 (1992). © 1992, American Chemical Society.

was very low (Fig. 12(A)), only a deformation of the reconstruction of the Au surface was observed, indicating the existence of a highly mobile molecular phase, i.e., 2D gas phase of the molecule. Ordered pin-stripe structures were observed at a slightly higher coverage (Fig. 12(B)). The period of the stripes was 2 times longer than the length of the molecule. Thus, a head-to-head molecular arrangement shown in Figure 13(β) was expected. The bright stripe line was formed by a thiol group and directed to the ⟨110⟩ direction, i.e., the next-nearest neighbor of gold atoms on the (111) surface. Alkyl chains were aligned along the ⟨101⟩ direction perpendicular to the stripe row.

As the coverage was increased (Fig. 12(C)), another kind of pin-stripe structure was formed. The period of the stripes was 2 times shorter than the molecular length, although the double bright line in STM images indicates two thiols

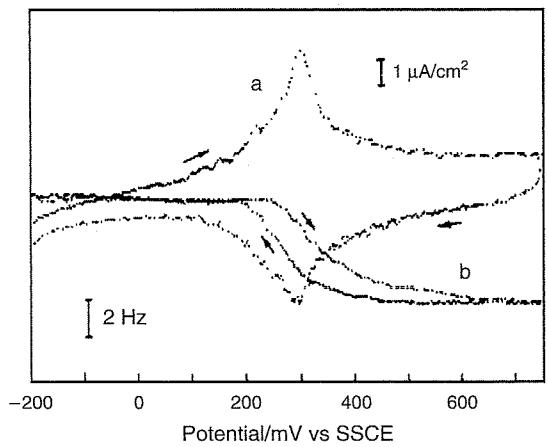

Figure 20. (a) Cyclic voltammogram of a Au electrode after the experiment shown in Figure 12 taken in 1 M $HClO_4$. (b) Frequency response during the potential sweep, showing the adsorption of anions on the $FcC_{11}SH$ SAM. Reprinted with permission from [100], K. Shimazu et al., *Langmuir* 8, 1385 (1992). © 1992, American Chemical Society.

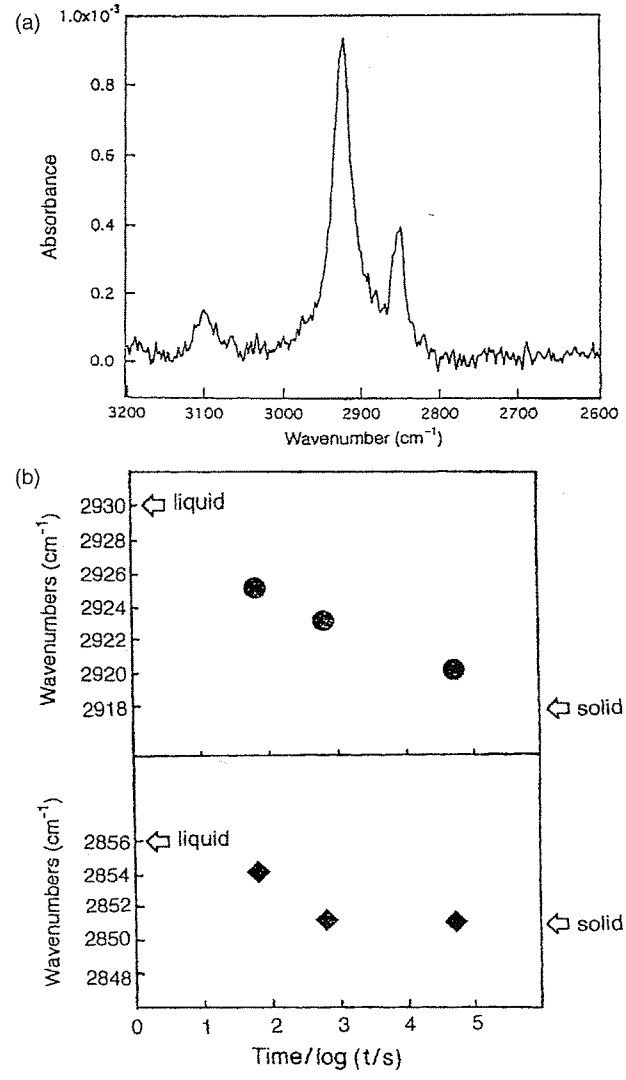

Figure 21. (a) CH stretching region of the PM-FTIR absorption spectrum of a $FcC_{11}SH$ monolayer on a gold electrode. Modification time was 10 min. (b) Evolution of peak positions of the methylene asymmetric (upper panel) and symmetric (lower panel) stretching modes. Reprinted with permission from [171], Y. Sato et al., *Bull. Chem. Soc. Jpn.* 67, 21 (1994). © 1994, American Chemical Society.

were coupled in a head-to-head configuration. Complex patterns with the same period were also found at higher coverage as shown in Figure 12(D, E). Plausible models for these structures are shown in Figure 13(χ, δ, and ϕ), in which the alkyl chains stack next to each other in rows. These structures are called interdigit structures. The phase behavior of an alkanethiol layer was investigated at various temperatures (Fig. 14).

A different model for the short pin stripe was proposed on the basis of AFM measurement [161]. Since protrusion between the stripes, which is expected for the interdigit structure, was not detected, a structure without stacking of alkyl chains was proposed. In this model, the direction of the alkyl chain is tilted from the row of stripes but still aligned along the NN direction of gold atoms on the (111) surface (Fig. 15).

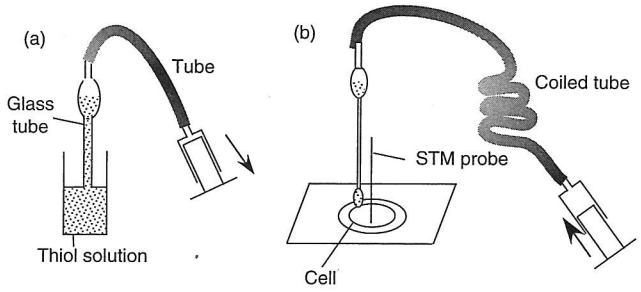

Figure 22. Experimental setup for the injection of decanethiol solutions in an STM cell. See text for details.

4.4. Molecular Arrangement of Thiol SAMs on a (100) Surface

Structures of SAMs of alkanethiols on a Au(100) surface have not been studied in detail. A Au(100) surface is known to be reconstructed, resulting in the formation of a hexagonal atomic arrangement as shown in Figure 16 [162].

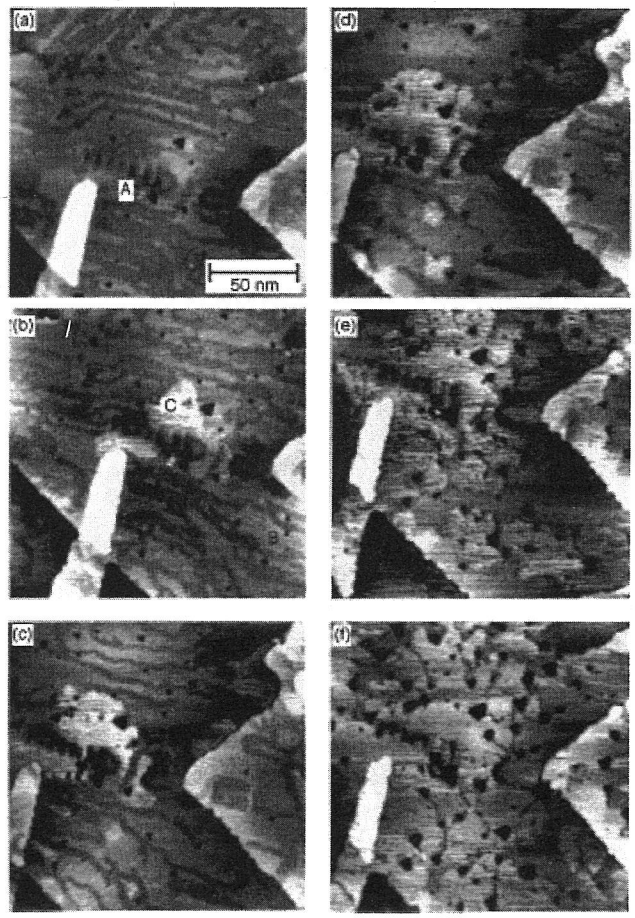

Figure 23. Sequential STM images of Au(111) taken in heptane solution: (a) 2 min after the first addition of the thiol solution; (b) 2 min and (c) 7 min after the second addition; (d) and (e) 2 and 12 min after the third addition; (f) 13 min after the fourth addition. The concentrations of the solution in the STM cell were ca. 0.1, 0.3, 0.5, and >0.5 μM after the first, second, third, and fourth additions of the solution. Reprinted with permission from [172], R. Yamada and K. Uosaki, *Langmuir* 14, 855 (1998). © 1998, American Chemical Society.

The reconstructed Au(100) surface shows periodic protrusions due to dislocations between the subsurface and the top-most layer [163].

STM investigation revealed that butanethiol molecules form a $c(2 \times 8)$ molecular lattice with 1×4 Au missing rows as shown in Figure 17 [164]. This structure is supported by GIXD [94, 165] measurement. However, another kind of structure, an incommensurate oblique cell, has also been reported [96, 166, 167].

In fact, both of these structures were observed on the Au(100) surface as shown in Figure 18 [168]. Adsorption of decanethiol on a reconstructed surface and a (1×1) surface resulted in the formation of $c(2 \times 8)$ and incommensurate oblique cell, respectively.

5. *IN SITU* OBSERVATION OF THE SA PROCESS

5.1. Introduction

Since formation of alkanethiol SAMs is usually carried out in solutions at room temperature, it is very important to follow the SA process in solutions *in situ* in real time. Solvents should affect the SA process, and the kinetics of molecular adsorption and surface pressure in the 2D phase of alkanethiols might be different from those in UHV conditions. These differences can result in the formation of different kinds of phases and SA process in solutions.

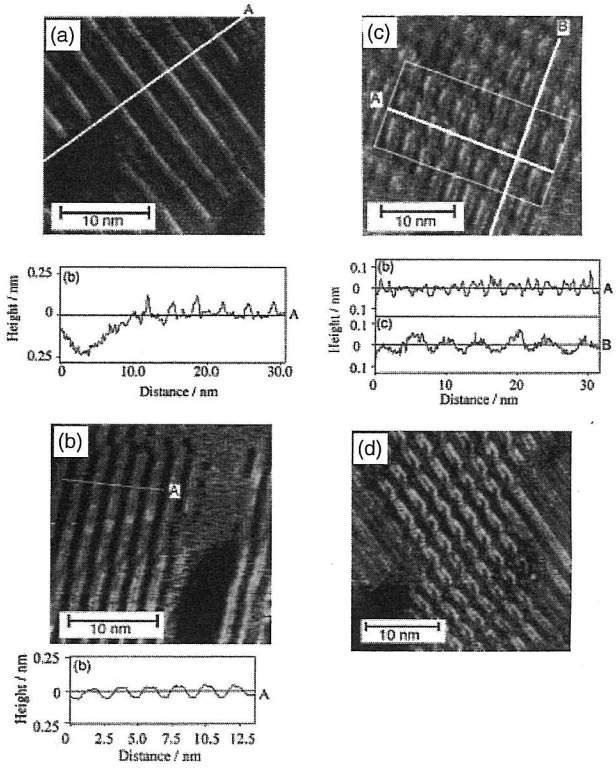

Figure 24. Various pin-stripe structures observed in dilute solution of decanethiol: (a) β–phase; (b), (c), and (d) δ–phase. Reprinted with permission from [172], R. Yamada and K. Uosaki, *Langmuir* 14, 855 (1998). © 1998, American Chemical Society.

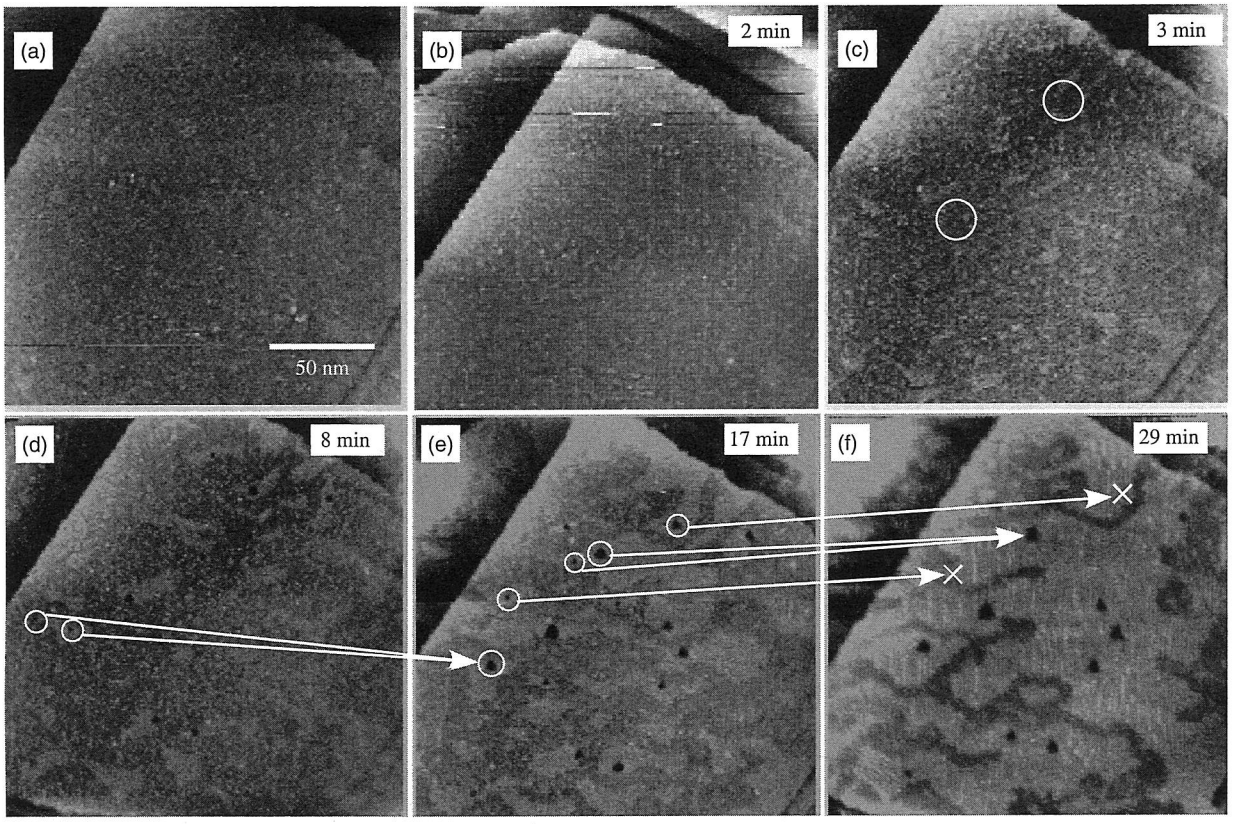

Figure 25. STM images of the Au(111) surface taken in ca. 0.1 μM solution of decanethiol. Circles show the locations where pits appeared. Some of the pits disappeared, while some of them seemed to have merged in the next image (shown by arrow between images). Reprinted with permission from [174], R. Yamada, Ph.D. Thesis, Hokkaido University (1999). © 1999.

In situ surface analytical methods in solutions have been developed and have progressed extensively in the last two decades [62]. Readers interested in techniques used for the analysis of the SAM formation process should refer to references [40, 169, 170].

5.2. Kinetics

We used QCM to study the kinetics of SAM formation *in situ* for the first time [100]. To monitor the SA process, a solution containing molecules was injected with stirring into a cell filled with pure hexane. As a control experiment, pure hexane was added (Fig. 19(a), dotted arrow). While the frequency of QCM temporally decreased by several hertz, it returned to the initial value within tens of seconds. Thus, the change in frequency due to addition of the liquid itself was negligible.

When a solution of 11-ferrocenyl-1-undecanethiol (FcC11SH) was added (Fig. 19(a) arrow, time = 0), the frequency decreased rapidly and then gradually with time. The frequency became constant about 800 s after the addition of the solution of FcC11SH. The total frequency change during the adsorption of FcC11SH was 9.0 Hz, which corresponds to 2.6×10^{14} molecules cm^{-2}. The number of molecules estimated from the charge used for the reaction of Fc/Fc^+ was 2.4×10^{14}, which is in good agreement with that expected from the frequency change (Fig. 20). This value is also consistent with the value, 2.7×10^{14}, that is expected from the model assuming that the diameter of Fc is 0.66 nm.

The initial fast and following slower steps were interpreted as a Langmuir-type adsorption of the molecules and healing process, respectively.

Ex situ IR measurement shows that the peak position of CH_2 vibration of the CH group gradually shifted to a lower frequency with immersion time in thiol solution, indicating gradual improvement of crystallinity of the film as shown in Figure 21 [171].

A multistep adsorption process was also observed for *n*-alkanethiols by other research groups [40, 169, 170]. Rate constants seem to be affected by subtle differences in experimental conditions such as stirring speed, cell structure, and crystallinity of the surface. Factors such as temperature, polarity of the solvent, solubility of the molecules, and functional group have not been systematically investigated.

5.3. Structural Evolution

In situ STM structural analysis of a SAM had been a challenge because of the difficulty in controlling coverage. This difficulty was overcome by gentle injection of very dilute solutions of alkanethiols during the scanning [172, 173].

Figure 21 shows an experimental setup. A glass tube with a bulge was prepared. The other end of the tube was connected to a soft and long silicone tube. The solution containing alkanethiols was sucked and stored in the bulge

of the tube by using a syringe connected to the other end of the silicone tube (Fig. 22(a)). Then the glass tube was fixed just above the STM cell.

A small droplet was generated at the tip of the glass tube and then injected into the cell containing pure solvent by pushing the syringe very gently (Fig. 22(b)). The soft silicone tube eliminates the mechanical vibrations caused by the operation of the syringe. The vibration of the liquid surface caused by the droplet injection disturbs only a few line scans in STM imaging. The droplets are sequentially injected to increase the coverage of the molecules on the surface in a step-by-step manner since the number of molecules contained in a single droplet is much less than that in a monolayer formation.

Evaporation of solvents is a problem in a long-term experiment. Heptane, which has a relatively small vapor pressure, was used as a solvent in the first *in situ* STM measurement by Yamada and Uosaki [172, 173]. The environmental atmosphere was saturated with heptane by putting a Petri dish filled with heptane in a sealed STM chamber.

Figure 23 shows experimental results. When droplets of 1 μM solution of decanethiol in heptane were injected, the bright thin lines were observed (Fig. 23(a), denoted A). The estimated concentration of thiol in the STM cell was ca. 0.1 μM. A magnified image of these regions showed the existence of pin-stripe patterns, i.e., the lying down phase of alkanethiols (Fig. 23(b), denoted B). These structures are discussed in detail later. VIs of the gold surface were also observed from the initial stage. As the coverage increased, elevated islands began to grow and covered the surface. They corresponded to the upright phase of alkanethiols since a $\sqrt{3} \times \sqrt{3}$ molecular arrangement was observed on these islands. Thus, the formation of the lying-down phase and following island-like growth of the upright phase were evident in solutions.

The pin-stripe structures were investigated in detail in dilute solutions. Various structures were observed on a surface. Figure 24(a) shows a stripe pattern with a period of 3.2 nm, which almost 2 times longer than the molecular length. In addition, the image revealed individual molecular structures in which alkyl chains were lying along the NN direction of the gold surface. This structure corresponds to the β–phase shown in Figure 13. The other pin-stripe structures shown in Figure 24(b–d) have a period of 2.3 nm. These structures correspond to the interdigit structure or the δ–phase shown in Figure 13.

The very initial stages of SA were investigated in very thin solutions to clarify the growth process of VIs as shown in Figure 25 [174]. When 0.1 μM solution of decanethiol was injected, small VIs were formed before ordered molecular structures were formed (arrow in Fig. 25(c)). Close inspection of the image revealed that small holes were created in and at the edges of the small islands, which would be the 2D liquid phase of alkanethiol. Some of the VIs seemed to coalesce with each other and become larger (Fig. 25(e, f)). Coalescence of VIs was also observed on the surface of low coverage in UHV [160] and in aqueous conditions [121]. Quantitative analysis of the number and area of VIs revealed that the growth process of VIs follows the Ostward-ripening model.

As mentioned before, temperature and solvent have strong effects on the size and number of domains and VIs [86, 87]. These effects are attributed to the difference in surface diffusion of alkanethiols and gold atoms at the very initial stage.

An interesting finding is that the disordered molecular islands suddenly changed into a pin-stripe structure (Fig. 25(e, f)). It is likely that phase transitions occurred during taking these images. This observation supports the phase behavior of alkanethiols similar to that in UHV conditions, i.e., surface pressure is required to form ordered phases.

VIs are known to disappear when alkanethiols are desorbed by thermal [175] or electrochemical [121] treatments. The desorption and readsorption of the alkanethols at the same location of the surface can be sequentially studied as shown in Figure 26 [121]. In the beginning, the potential of the electrode was set to −1000 mV to remove the hexanethiol monolayer. Then the potential was positively swept (Fig. 26(a)). White arrows in the images are pointers showing the identical position of the surface. Initially, the gold surface showed local reconstruction as denoted by black arrows in Figure 26(a), suggesting that no molecules existed on the surface at this potential. As the potential became positive, the reconstruction disappeared and VIs appeared. The monolayer formation was completed when the potential of the electrode was −450 mV (Fig. 26(e)).

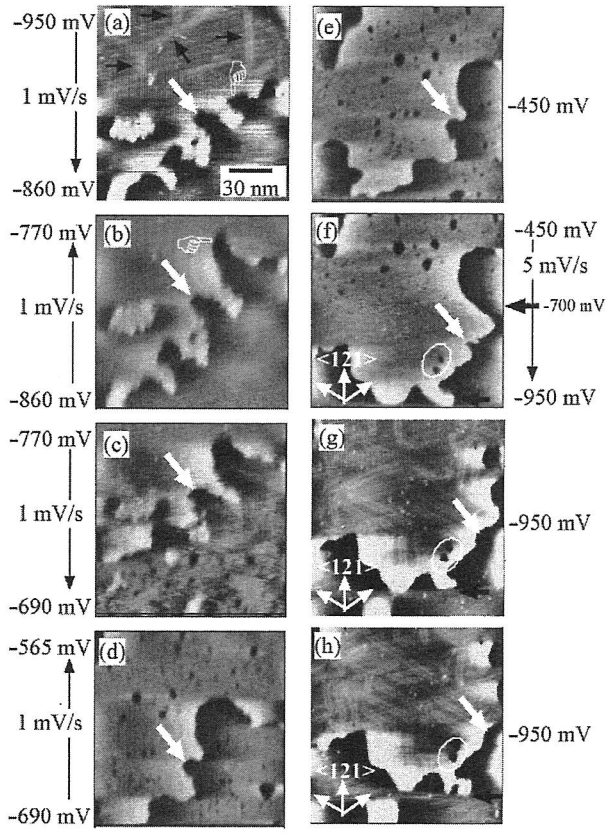

Figure 26. *In situ* STM images of a Au(111) electrode in 20 mM KOH ethanol solution containing 60 μM hexanethiol. All images were sequentially taken. Arrows beside the image indicate the frame direction of STM. A hexanethiol monolayer is known to desorb around −800 mV. Oxidative adsorption of desorbed molecules took place around −700 mV. Reprinted with permission from [121], H. Wano and K. Uosaki, *Langmuir* 21, 4024 (2005). © 2005, American Chemical Society.

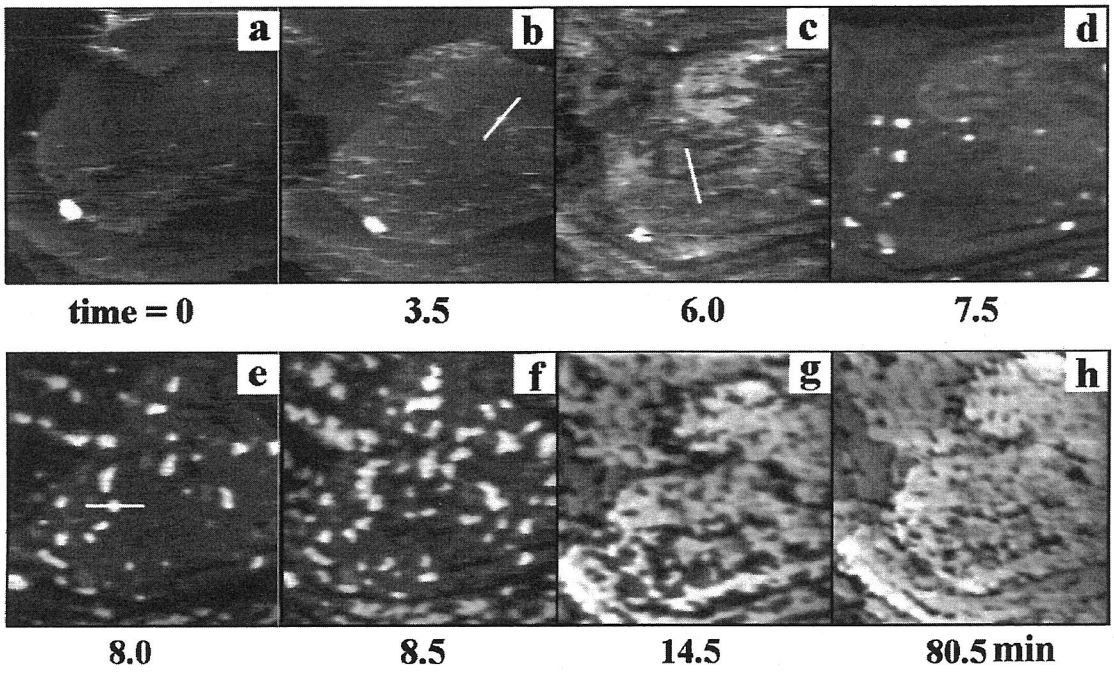

Figure 27. AFM images of the Au(111) surface after injection of a solution of octadecanethiol in 2-butanol. The concentration of octadecanethiol in the AFM cell was 0.2 mM. Reprinted with permission from [177], S. Xu et al., *J. Chem. Phys.* 108, 5002 (1998). © 1998, American Chemical Society.

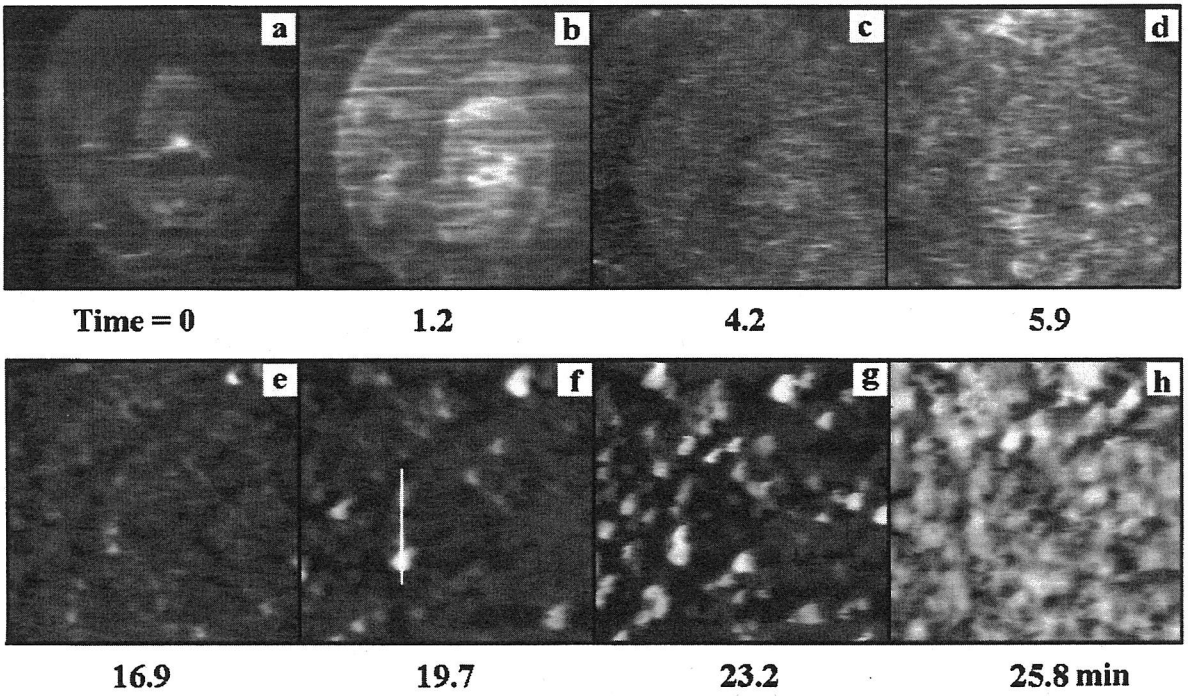

Figure 28. AFM images of the Au(111) surface taken in 0.2 μM solution of C_{18}-O-C_{19}SH. The cross section along the line (f) is shown in Figure 29. Reprinted with permission from [177], S. Xu et al., *J. Chem. Phys.* 108, 5002 (1998). © 1998, American Chemical Society.

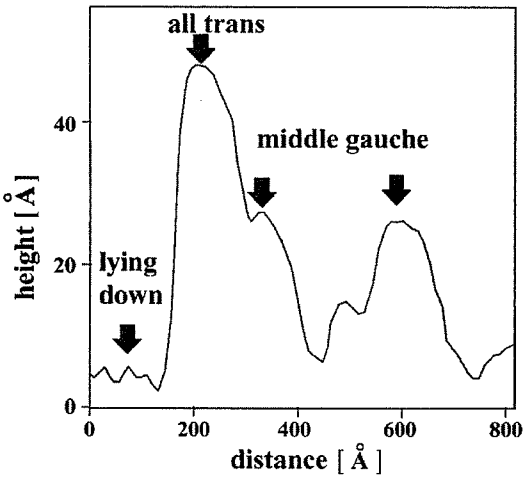

Figure 29. Cross section of the image shown in Figure 28(f). Reprinted with permission from [177], S. Xu et al., *J. Chem. Phys.* 108, 5002 (1998). © 1998, American Chemical Society.

The potential was then negatively swept again. The VIs suddenly disappeared and reconstruction of the Au(111) surface was reformed Figure 26(f, g). During the adsorption and desorption of thiols, the structure of the gold atomic step changed greatly as evident at the place indicted by the finger. This observation indicates that the gold atoms moved a lot during the adsorption and desorption of alkanethiols.

An interesting finding is that VIs remained even after the desorption of thiolate in KOH aqueous solution despite the fact that reconstruction of Au(111) was rebuild [176]. This phenomenon may be explained by considering the mobility of gold atoms on the surface. In addition to gold atoms to fulfill VIs, an excess amount of gold atoms should be taken in to the fist surface layer to construct the $\sqrt{3} \times 23$ structure. The gold atoms were probably supplied from nearby steps, and, thus, kinetics of the gold atom diffusion process should have a strong influence on the surface morphology after the desorption of thiolate.

The structural evolutions of alkanethiols of longer alkyl chains, $CH_3(CH_2)_{17}SH$ and $CH_3(CH_2)_{17}O(CH_2)_{19}SH$, were investigated by AFM in solutions as shown in Figures 27 and 28, respectively [177]. Although pin-stripe phases were not observed, islands with a height of molecular diameter were observed during the growth of the $CH_3(CH_2)_{17}SH$ monolayer as shown in Figure 27. These islands corresponded to the lying-down phase of alkanethiols. As adsorption proceeded, elevated islands began to appear. The height of the islands corresponded to that expected for the upright phase. Thus, the structural evolution is basically the same with alkanethiols of shorter chain length.

AFM observations of the adsorption of $CH_3(CH_2)_{17}O(CH_2)_{19}SH$ revealed a kind of healing process of alkyl chains (Fig. 28). In an AFM image of the intermediate state of the monolayer formation, two kinds of elevated islands were observed above the lying-down phase as shown in Figure 29. The lower islands were attributed to molecules with gauche defect at the ether unit. As adsorption proceed, the higher islands dominated the surface, indicating that the gauche defect at the ether was extended.

There seems to be a disagreement between results of structural and kinetic studies. Structural analysis has clearly shown that the island growth although a Langmuir isotherm, i.e., random adsorption onto vacancy site, explains the kinetics observed in most of the adsorption processes. One of the conditions not take into account in analysis of kinetic data is the high mobility of molecules on the surface, especially in the flat-lying phase. A model including surface diffusion should be developed to interpret the kinetics.

6. SUMMARY

In situ and *ex situ* analyses have revealed the SA process of alkanethiol on a Au(111) surface with molecular resolutions. At low coverage, the metal-molecule interactions dominate the molecular orientation and, thus, molecules are lying down on the surface. The alkanethiols form ordered structures called pin-stripe phases at this stage. The up-right phases grow after the surface is completely covered with pin-stripes phases. These findings indicate that the formation of a monolayer is a result of high pressure on the surface rather than a result of strong lateral interactions among the alkyl chains. Gold atoms are also highly mobile and extracted from the surface, leaving VIs on the gold surface.

The basic aspects of the structure of SAMs, such as the position of sulfur and origin of VIs, are not fully understood yet, though alkanethiol SAMs are likely to be one of the most well-controlled and simplest systems. One of the difficulties may come from the complexity of the surface reaction itself. The gold surface itself possesses unique characteristics such as reconstruction. Not only charge transfer but also lifting of reconstruction, i.e., the rearrangement of the atoms in the surface layer, takes place. More precise measurement and theoretical understanding are required to obtain the complete picture of the monolayer and its formation process.

REFERENCES

1. G. A. Somorjai, "Introduction to Surface Chemistry and Catalysis." Wiley-Interscience, New York, 1993.
2. A. Zangwill, "Physics at Surfaces." Cambridge University Press. Cambridge, 1988.
3. A. Ulman, "An Introduction to Ultrathin Organic Films from Langmuir-Blodgett to Self-Assembly." Academic Press, San Diego, 1991.
4. A. Ulman, *Chem. Rev.* 96, 1533 (1996).
5. P. E. Laibinis, G. M. Whitesides, D. L. Allara, Y. T. Tao, A. N. Parikh, and R. G. Nuzzo, *J. Am. Chem. Soc.* 113, 7152 (1991).
6. O. M. Magnussen, B. M. Ocko, M. Deutsch, M. J. Regan, R. S. Pershan, D. Abernathy, G. Grubel, and J. F. Legrand, *Nature* 384, 250 (1996).
7. T. Baum, S. Ye, and K. Uosaki, *Langmuir* 15, 8577 (1999).
8. Y. Sato and K. Uosaki, *J. Electroanal. Chem.* 384, 57 (1995).
9. T. Kondo, M. Takechi, Y. Sato, and K. Uosaki, *J. Electroanal. Chem.* 381, 203 (1995).
10. L. V. Protsailo, W. R. Fawcett, D. Russell, and R. L. Meyer, *Langmuir* 18, 9342 (2002).
11. Y. Sato and F. Mizutani, *Phys. Chem. Chem. Phys.* 6, 1328 (2004).
12. J. D. Monnell, J. J. Stapleton, J. J. Jackiw, T. Dunbar, W. A. Reinerth, S. M. Dirk, J. M. Tour, D. L. Allara, and P. S. Weiss, *J. Phys. Chem. B* 108, 9834 (2004).

13. X. Li and A. A. Gewirth, *J. Am. Chem. Soc.* 125, 11674 (2003).
14. D. S. Corrigan, J. K. Foley, P. Gao, S. Pons, and M. J. Weaver, *Langmuir* 1, 616 (1985).
15. L. Netzer and J. Sagiv, *J. Am. Chem. Soc.* 105, 674 (1983).
16. J. Quinton, L. Thomsen, and P. Dastoor, *Surf. Interface Anal.* 25, 931 (1997).
17. D. G. Kurth and T. Bein, *Langmuir* 11, 3061 (1995).
18. K. M. Chen, W. B. Caldwell, and C. A. Mirkin, *J. Am. Chem. Soc.* 115, 1193 (1993).
19. M. R. Linford, P. Fenter, P. M. Eisenberger, and C. E. D. Chidsey, *J. Am. Chem. Soc.* 117, 3145 (1995).
20. W. Cai, Z. Lin, T. Strother, L. M. Smith, and R. J. Hamers, *J. Phys. Chem. B* 106, 2656 (2002).
21. K. Choi and J. M. Buriak, *Langmuir* 16, 7737 (2000).
22. H. Z. Yu, S. Morin, D. D. M. Wayner, P. Allongue, and C. H. de Villeneuve, *J. Phys. Chem. B* 104, 11157 (2000).
23. A. Bansal, X. L. Li, I. Lauermann, N. S. Lewis, S. I. Yi, and W. H. Weinberg, *J. Am. Chem. Soc.* 118, 7225 (1996).
24. A. Bansal and N. S. Lewis, *J. Phys. Chem. B* 102, 4058 (1998).
25. A. Bansal and N. S. Lewis, *J. Phys. Chem. B* 102, 1067 (1998).
26. G. W. Cullen, J. A. Amick, and D. Gerlich, *J. Electrochem. Soc.* 109, 124 (1962).
27. J. A. Amick, G. W. Cullen, and D. Gerlich, *J. Electrochem. Soc.* 109, 127 (1962).
28. D. Gerlich, G. W. Cullen, and J. A. Amick, *J. Electrochem. Soc.* 109, 133 (1962).
29. J. L. He, Z. H. Lu, S. A. Mitchell, and D. D. M. Wayner, *J. Am. Chem. Soc.* 120, 2660 (1998).
30. J. H. Song and M. J. Sailor, *J. Am. Chem. Soc.* 120, 2376 (1998).
31. J. H. Song and M. J. Sailor, *Inorg. Chem.* 38, 1498 (1999).
32. P. Allongue, C. H. de Villeneuve, G. Cherouvrier, R. Cortes, and M. C. Bernard, *J. Electroanal. Chem.* 550, 161 (2003).
33. J. J. Hickman, P. E. Laibinis, D. I. Auerbach, C. F. Zou, T. J. Gardner, G. M. Whitesides, and M. S. Wrighton, *Langmuir* 8, 357 (1992).
34. D. H. Kang and M. Trenary, *J. Am. Chem. Soc.* 123, 8432 (2001).
35. K. L. Murphy, W. T. Tysoe, and D. W. Bennett, *Langmuir* 20, 1732 (2004).
36. J. C. Love, L. A. Estroff, J. K. Kriebel, R. G. Nuzzo, and G. M. Whitesides, *Chem. Rev.* 105, 1103 (2005).
37. R. G. Nuzzo and D. L. Allara, *J. Am. Chem. Soc.* 105, 4481 (1983).
38. A. Ulman, "Self-Assembled Monolayers of Thiols." Academic Press, San Diego, 1998.
39. F. Schreiber, *J. Phys.: Condens. Matter.* 16, R881 (2004).
40. F. Schreiber, *Prog. Surf. Sci.* 65, 151 (2000).
41. F. Schreiber, *Annu. Rev. Phys. Chem.* 52, 107 (2001).
42. G. E. Poirier, *Chem. Rev.* 97, 1117 (1997).
43. C. Vericat, M. E. Vela, and R. C. Salvarezza, *Phys. Chem. Chem. Phys.* 7, 3258 (2005).
44. G. E. Poirier and M. J. Tarlov, *Science* 272, 1145 (1996).
45. H. Kondoh, C. Kodama, H. Sumida, and H. Nozoye, *J. Chem. Phys.* 111, 1175 (1999).
46. R. Thomas, L. Sun, and R. M. Crooks, *Langmuir* 7, 620 (1991).
47. M. Godin, P. J. Williams, V. Tabard-Cossa, O. Laroche, L. Y. Beaulieu, R. B. Lennox, and P. Grxtter, *Langmuir* 20, 7090 (2004).
48. A. L. Deering, S. M. Van Lue, and S. A. Kandel, *Langmuir* 21, 10263 (2005).
49. P. E. Laibinis and G. M. Whitesides, *J. Am. Chem. Soc.* 114, 1990 (1992).
50. N. L. Abbott, C. B. Gorman, and G. M. Whitesides, *Langmuir* 11, 16 (1995).
51. S. Abbott, J. Ralston, G. Reynolds, and R. Hayes, *Langmuir* 15, 8923 (1999).
52. K. Ichimura, S. K. Oh, and M. Nakagawa, *Science* 288, 1624 (2000).
53. J. Lahann, S. Mitragotri, T. N. Tran, H. Kaido, J. Sundaram, U. S. Choi, S. Hoffer, G. A. Somorjai, and R. Langer, *Science* 299, 371 (2003).
54. R. Yamada and H. Tada, *Langmuir* 21, 4254 (2005).
55. A. J. Bard and L. R. Faulkner, "Electrochemical Methods: Fundamentals and Applications," 2nd edn. John Wiley & Sons, Inc., 2001.
56. C. E. D. Chidsey, *Science* 251, 919 (1991).
57. K. Uosaki, Y. Sato, and H. Kita, *Langmuir* 7, 1510 (1991).
58. D. M. Collard and M. A. Fox, *Langmuir* 72, 1192 (1991).
59. G. K. Rowe and S. E. Greager, *Langmuir* 7, 2307 (1991).
60. K. Uosaki, T. Kondo, X.-Q. Zhang, and M. Yanagida, *J. Am. Chem. Soc.* 119, 8367 (1997).
61. B. Ohtani, A. Shinani, and K. Uosaki, *J. Am. Chem. Soc.* 121, 6515 (1999).
62. A. A. Gewirth and H. Siegenthaler, eds., "Nanoscale Probes of the Solid/Liquid Interface." Springer, New York, 1995.
63. K. Reichelt and H. O. Lutz, *J. Cryst. Growth* 10, 103 (1971).
64. C. E. D. Chidsey, D. N. Loiacono, T. Sleator, and S. Nakahara, *Surf. Sci.* 200, 45 (1988).
65. C. A. Lang, M. M. Dovek, J. Nagami, and C. F. Quate, *Surf. Sci.* 224, L947 (1989).
66. E. Holland-Moritz, J. H. Gordon, G. Borges, and R. Sonnenfeld, *Langmuir* 7, 301 (1991).
67. M. S. Zei, Y. Nakai, G. Lehmpfuhl, and D. M. Kolb, *J. Electroanal. Chem.* 150, 201 (1983).
68. D. Hecht and D. Stark, *Thin Solid Films* 238, 258 (1994).
69. K. Uosaki, Y. Shen, and T. Kondo, *J. Phys. Chem.* 99, 14117 (1995).
70. M. Josowicz, J. Janata, and M. Levy, *J. Electrochem. Soc.* 135, 112 (1988).
71. T. C. Tisone and J. Drovek, *J. Vaccum Sci. Technol.* 9, 271 (1972).
72. G. W. B. Ashwell and R. J. Heckingbottom, *J. Electrochem. Soc.* 128, 649 (1981).
73. P. H. Holloway, *Gold Bull.* 12, 99 (1978).
74. J. J. Ponjee, J. W. A. Nelissen, and C. J. A. Verwijlen, *Eur. Pat. Appl. EP* 111, 957 (1984).
75. D. L. Allara, A. F. Hebard, F. J. Padden, R. G. Nuzzo, and D. R. Falcone, *J. Vaccum Sci. Technol. A* 1, 376 (1983).
76. S. R. Wasserman, H. Biebuyck, and G. M. Whitesides, *J. Mater. Res.* 3, 886 (1989).
77. C. A. Goss, D. H. Charych, and M. Majda, *Anal. Chem.* 63, 85 (1991).
78. J. Clavilier, *J. Electroanal. Chem.* 107, 211 (1980).
79. J. Clavilier, *J. Electroanal. Chem.* 107, 205 (1980).
80. K. Uosaki, S. Ye, H. Naohara, Y. Oda, T. Haba, and T. Kondo, *J. Phys. Chem. B* 101, 7566 (1997).
81. H. Naohara, S. Ye, and K. Uosaki, *J. Phys. Chem. B* 102, 4366 (1998).
82. H. Naohara, S. Ye, and K. Uosaki, *J. Electroanal. Chem.* 473, 2 (1999).
83. L. A. Kibler, A. M. El-Aziz, and D. M. Kolb, *J. Mol. Catal. A* 199, 57 (2003).
84. I. Taniguchi, S. Yoshimoto, M. Yoshida, S. Kobayashi, T. Miyawaki, Y. Aono, Y. Sunatsuki, and H. Taira, *Electrochem. Acta* 45, 2843 (2000).
85. M. Abe, T. Michi, A. Sato, T. Kondo, W. Zhou, S. Ye, K. Uosaki, and Y. Sasaki, *Angew. Chem. Int. Ed.* 42, 2912 (2003).
86. R. Yamada, H. Wano, and K. Uosaki, *Langmuir* 16, 5523 (2000).
87. R. Yamada, H. Sakai, and K. Uosaki, *Chem. Lett.* 28, 667 (1999).
88. C. D. Bain, E. B. Troughton, Y.-T. Tao, J. Evall, G. M. Whitesides, and R. G. Nuzzo, *J. Am. Chem. Soc.* 111, 321 (1989).
89. R. G. Nuzzo, E. M. Korenic, and L. H. Dubois, *J. Chem. Phys.* 93, 767 (1990).
90. K. A. Peterlinz and R. Georgiadis, *Langmuir* 12, 4731 (1996).
91. R. F. DeBono, G. D. Loucks, M. D. Della, and U. J. Krull, *Can. J. Chem.* 74, 677 (1996).

92. K. Tamada. M. Hara, H. Sasabe, and W. Knoll, *Langmuir* 13, 1558 (1997).
93. T. Kondo, M. Yanagida, K. Shimazu, and K. Uosaki, *Langmuir* 14, 5656 (1998).
94. P. Fenter, X-ray and He Atom Diffraction Studies of Self-Assembled Monolyaers, "Self-Assembled Monolayers of Thiols" (A. Ulman, ed.), Vol. 24. *Thin Films* (1998).
95. P. Fenter, A. Eberhardt, and P. Eisenberger, *Science* 266, 1216 (1994).
96. L. H. Dubois, B. R. Zegarski, and R. G. Nuzzo, *J. Chem. Phys.* 98, 678 (1993).
97. E. Delamarche, B. Michel, Ch. Gerber, D. Anselmetti, H. J. Gxntherodt, H. Wolf, and H. Ringsdorf, *Langmuir* 10, 2869 (1994).
98. G. E. Poirier and M. J. Tarlov, *Langmuir* 10, 2853 (1994).
99. C. A. Widrig, C. Chung, and M. D. Porter, *J. Electroanal. Chem.* 310, 335 (1991).
100. K. Shimazu, I. Yagi, U. Sato, and K. Uosaki, *Langmuir* 8, 1385 (1992).
101. D. S. Karpovich and G. J. Blanchard, *Langmuir* 10, 3315 (1994).
102. K. Tamada, M. Hara, H. Sasabe, and W. Knoll, *Langmuir* 13, 1558 (1997).
103. A. W. Adamson and A. P. Gast, "Physical Chemistry of Surfaces," 6th edn. Wiley-Interscience, New York, 1997.
104. A. Ishitani, H. Ishida, F. Soeda, and Y. Nagasawa, *Anal. Chem.* 54, 682 (1982).
105. J. F. Blanke, S. E. Vincent, and J. Overend, *Spectrochim. Acta, Part A* 32, 163 (1976).
106. G. L. Gaines, Jr., "Insoluble Monolayers at Liquid-Gas Interfaces." Interscience, New York, 1966.
107. A. E. Dowry and C. Marcott, *Appl. Spectrosc.* 36, 414 (1982).
108. W. G. Golden, K. Kunimatsu, and H. Seki, *J. Phys. Chem.* 88, 1275 (1984).
109. K. Kunimatsu, W. G. Golden, H. Seki, and M. R. Philpott, *Langmuir* 1, 245 (1985).
110. G. L. Haller and R. W. Rice, *J. Phys. Chem.* 74, 4386 (1970).
111. R. Mao and J. Sagiv, *J. Colloid. Interface Sci.* 100, 465 (1984).
112. M. D. Porter, T. B. Bright, D. L. Allara, and C. E. D. Chidsey, *J. Am. Chem. Soc.* 109, 3559 (1987).
113. Y. R. Shen, *Proc. Natl. Acad. Sci. U.S.A.* 93, 12104 (1996).
114. C. D. Bain, *J. Chem. Soc., Faraday Trans.* 91, 1281 (1995).
115. P. B. Miranda and Y. R. Shen, *J. Phys. Chem. B* 103, 3292 (1999).
116. M. Zharnikov and M. Grunze, *J. Vac. Sci. Technol. B* 20, 1793 (2002).
117. C. J. Chen, "Introduction to Scanning Tunneling Microscopy." Oxford University Press, New York, 1993.
118. R. Wiesendanger, "Scanning Probe Microscopy and Spectroscopy: Methods and Applications." Cambridge University Press, UK, 1994.
119. D. Bonnell, ed., "Scanning Probe Microscopy and Spectroscopy: Theory, Techniques, and Applications," 2nd edn. Wiley-VCH, New York, 2000.
120. H. J. Guntherodt and R. Wiesendanger, eds., "Scanning Tunneling Microscopy I: General Principles and Applications to Clean and Absorbate-Covered Surfaces," 2nd edn. Springer, New York, 1994.
121. H. Wano and K. Uosaki, *Langmuir* 21, 4024 (2005), and references therein.
122. D. A. Buttry and M. D. Ward, *Chem. Rev.* 92, 1355 (1992).
123. A. Janshoff, H.-J. Galla, and C. Steinem, *Angew. Chem. Int. Ed.* 39, 4004 (2000).
124. E. Hwang and Y. Lim, *Bull. Korean. Chem. Soc.* 17, 39 (1996).
125. H. O. Finklea, "Electroanalytical Chemistry" (A. J. Bard and I. Rubinstein, eds.), Vol. 19, p. 109. Dekker, New York, 1999.
126. S. E. Creager and K. G. Olsen, *Anal. Chim. Acta* 307, 277 (1995).
127. J. A. M. Sondag-Huethorst and L. G. J. Fokkink, *J. Electroanal. Chem.* 367, 49 (1994).
128. R. Haneda, H. Nishihara, and K. Aramaki, *J. Electrochem. Soc.* 144, 1215 (1997).
129. C. E. D. Chidsery, C. R. Betrozzi, T. M. Putvinski, and A. M. Mujsce, *J. Am. Chem. Soc.* 112, 4301 (1990).
130. S. Ye, T. Haba, U. Sato, K. Shimazu, and K. Uosaki, *Phys. Chem. Chem. Phys.* 1, 3653 (1999).
131. R. C. Chambers, C. E. Inman, and J. E. Hutchison, *Langmuir* 21, 4615 (2005).
132. B. Kazakevicienê, G. Valincius, G. Niaura, Z. Talaikytê, M. Kažemêkaitê, and V. Razumas, *J. Phys. Chem. B* 107, 6661 (2003).
133. C. E. D. Chidsey and D. N. Loiacono, *Langmuir* 6, 682 (1990).
134. N. Camillone, C. E. D. Chidsey, G.-Y. Liu, and G. Scoles, *J. Chem. Phys.* 98, 3503 (1993).
135. P. Fenter, P. Eisenberger, and K. S. Liang, *Phys. Rev. Lett.* 70, 2447 (1993).
136. K. Edinger, A. Golzhauser, K. Demota, C. Woll, and M. Grunze, *Langmuir* 9, 4 (1993).
137. C. Schoenenberger, J. A. M. Sondag-Huethorest, J. Jorritsma, and L. G. J. Fokkink, *Langmuir* 10, 611 (1994).
138. C. A. McDermott, M. T. McDermott, J. B. Green, and M. D. Porter, *J. Phys. Chem.* 99, 13257 (1995).
139. J. Noh and H. Hara, *Langmuir* 18, 1953 (2002).
140. T. Fukuda, T. Ichii, K. Kobayashi, H. Yamada, and K. Matsushige, *J. Appl. Phys.* 95, 1222 (2004).
141. T. Fukuda, T. Ichii, K. Kobayashi, H. Yamada, and K. Matsushige, *Appl. Phys. Lett.* 86, 034103 (2005).
142. M. G. Roper, M. P. Skegg, C. J. Fisher, J. J. Lee, V. R. Dhanak, D. P. Woodruff, and R. G. Jones, *Chem. Phys. Lett.* 389, 87 (2004).
143. H. Kondoh, M. Iwasaki, T. Shimada, K. Amemiya, T. Yokohama, T. Ohta, M. Shimomura, and S. Kondo, *Phys. Rev. Lett.* 90, 066102 (2003).
144. T. Kitagawa, Y. Idomoto, H. Matsubara, D. Hobara, T. Kakiuchi, T. Okazki, and K. Komatsu, *J. Org. Chem.* 71, 1362 (2006).
145. T. Hayashi, Y. Morikawa, and H. Nozoye, *J. Chem. Phys.* 114, 7615 (2001).
146. M. C. Vargas, P. Giannozzi, A. Selloni, and G. Scoles, *J. Phys. Chem. B* 105, 9509 (2001).
147. J. Gottschalck and B. Hammer, *J. Chem. Phys.* 116, 784 (2002).
148. M. L. Molina and B. Hammer, *Chem. Phys. Lett.* 360, 264 (2002).
149. J. Nara, S. Higai, Y. Morikawa, and T. Ohno, *J. Chem. Phys.* 120, 6705 (2004).
150. P. Fenter, F. Schreiber, L. Berman, P. Scoles, P. Eisenberger, and M. Bedzyk, *Surf. Sci.* 412/413, 213 (1998).
151. P. Fenter, F. Schreiber, L. Berman, P. Scoles, P. Eisenberger, and M. Bedzyk, *Surf. Sci.* 425, 138 (1999).
152. X. Torrelles, E. Barrena, C. Munuera, J. Rius, S. Ferrer, and C. Ocal, *Langmuir* 20, 9396 (2004).
153. F. Teran Arce, M. E. Vela, R. C. Salvarezza, and A. J. Arvia, *J. Chem. Phys.* 109, 5703 (1998).
154. X. Torrelles, C. Vericat, M. E. Vela, M. H. Fonticelli, M. A. D. Millone, R. Felici, T. L. Lee, J. Zegenhagen, G. Munoz, J. A. Martin-Gago, and R. C. Salvarezza, *J. Phys. Chem. B* 110, 5586 (2006).
155. G. E. Poirier and M. J. Tarlov, *J. Phys. Chem.* 99, 10966 (1995).
156. O. Cavallcri, A. Hirstein, and K. Kern, *Surf. Sci.* 341, L960 (1995).
157. G. E. Poirier, *Langmuir* 13, 2019 (1997).
158. O. Cavalleri, A. Hirstein, J. P. Bucher, and K. Kern, *Thin Solid Films* 284–285, 392 (1996).
159. O. Cavalleri, S. E. Gilbert, and K. Kern, *Chem. Phys. Lett.* 269, 479 (1997).
160. G. E. Poirier, W. P. Fitts, and J. M. White, *Langmuir* 17, 1176 (2001).
161. C. Munuera, E. Barrena, and C. Ocal, *Langmuir* 21, 8270 (2005).
162. O. M. Magnussen, J. Hotlos, R. K. Behm, N. Batina, and D. M. Kolb, *Surf. Sci.* 296, 310 (1993).
163. D. M. Kolb, *Prog. Surf. Sci.* 51, 109 (1996).
164. G. E. Poirier, *J. Vaccum Sci. Technol. B* 14, 1453 (1996).

165. J. Li, K. S. Liang, N. Camillone, III, T. Y. B. Leung, and G. Scoles, *J. Chem. Phys.* 102, 5012 (1995).
166. L. Strong and G. M. Whitesides, *Langmuir* 4, 546 (1988).
167. N. Camillone, III, C. E. D. Chidsery, G. Liu, and G. Scoles, *J. Chem. Phys.* 98, 4234 (1993).
168. R. Yamada and K. Uosaki, *Langmuir* 17, 4148 (2001).
169. D. K. Schwartz, *Annu. Rev. Phys. Chem.* 52, 107 (2001).
170. N. Camillone, III, *Langmuir* 20, 1199 (2004).
171. Y. Sato, B. L. Fray, R. M. Corn, and K. Uosaki, *Bull. Chem. Soc. Jpn.* 67, 21 (1994).
172. R. Yamada and K. Uosaki, *Langmuir* 14, 855 (1998).
173. R. Yamada and K. Uosaki, *Langmuir* 13, 5218 (1997).
174. R. Yamada, Ph.D. Thesis, Hokkaido University, 1999.
175. N. Camillone, III, P. Eisenberger, T. Y. B. Leung, P. Schwartz, G. Scoles, G. E. Poirier, and M. J. Tarlov, *J. Chem. Phys.* 101, 11 031 (1994).
176. H. Wano and K. Uosaki, *Langmuir* 17, 8227 (2005).
177. S. Xu, S. J. N. Cruchon-Dupeyrat, J. C. Garno, G.-Y. Liu, G. K. Jennings, T.-H. Yong, and P. E. Laibinis, *J. Chem. Phys.* 108, 5002 (1998).